
Mechanistic Interpretability with Sparse Autoencoder Neural Operators

Bahareh Tolooshams^{*123} Ailsa Shen^{*4} Anima Anandkumar⁴

Abstract

We introduce sparse autoencoder neural operators (SAE-NOs), a new class of sparse autoencoders that operate directly in infinite-dimensional function spaces. We generalize the linear representation hypothesis to a functional representation hypothesis, enabling concept learning beyond vector-valued representations. Unlike standard SAEs that employ multi-layer perceptrons (SAE-MLP) to each concept with a scalar activation, we introduce and formalize sparse autoencoder neural operators (SAE-NOs), which extend vector-valued representations to functional ones. We instantiate this framework as SAE Fourier neural operators (SAE-FNOs), parameterizing concepts as integral operators in the Fourier domain. We show that this functional parameterization fundamentally shapes learned concepts, leading to improved stability with respect to sparsity level, robustness to distribution shifts, and generalization across discretizations. We show that SAE-FNO is more efficient in concept utilization across data population and more effective in extracting localized patterns from data. We show that convolutional SAEs (SAE-CNNs) do not generalize their sparse representations to unseen input resolutions, whereas SAE-FNOs operate across resolutions and reliably recover the underlying representations. Our results demonstrate that moving from fixed-dimensional to functional representations extends sparse autoencoders from detectors of concept presence to models that capture the underlying structure of the data, highlighting parameterization as a central driver of interpretability and generalization.

1. Introduction

Sparse autoencoders (SAEs) (Makhzani & Frey, 2014) are popular in machine learning for learning structured and interpretable representations (Huben et al., 2023). More broadly, sparse representations are widely used for representation learning (Bengio et al., 2013), providing a mathematically grounded framework for uncovering parsimonious latent structure through interpretable components.

SAEs have increasingly become a tool for understanding model capabilities and internal representations themselves (Doshi-Velez & Kim, 2017). In this context, SAEs are widely used for mechanistic interpretability (Bricken et al., 2023a), where the goal is to explain model behaviour by identifying the internal concepts and representations that drive computation in large neural networks. The linear representation hypothesis (LRH) postulates that internal activations can be decomposed into orthogonal concepts. Hence, SAEs are primarily designed under this hypothesis to decompose activations into linearly accessible and approximately orthogonal concepts that can be sparsely and linearly combined to represent the data (Elhage et al., 2022).

LRH directly motivates the use of a shallow SAEs, where the learned decoder weights encapsulate the dictionary of interpretable concepts. This hypothesis has been supported by numerous empirical analyses on the geometry of concepts captured by internal representations of large models (Fel et al., 2023; Merullo et al., 2025). Given this hypothesis, the architecture of almost all SAEs for interpretability has shallow non-linear multi-layer perceptron (MLP) encoder and shallow linear decoder, as we term this as SAE-MLP, hence differing primarily on their choice on the encoder nonlinearity (Bussmann et al., 2025; Hindupur et al., 2025).

While SAE-MLPs have proven effective for sparse model recovery (Olshausen & Field, 1996) and identifying monosemantic features (Bricken et al., 2023b), their architectural design inherently limits what a concept can represent. They all share three fundamental properties: i) concept utilization is summarized by a scalar activation, encoding presence and strength, but no further structure, ii) concepts are parameterized in the same domain as the inputs, and iii) the inference of sparse representation and the learning of concepts happen in Euclidean spaces with a fixed discretization sampling.

¹University of Alberta ²Alberta Machine Intelligence Institute (Amii) ³Neuroscience and Mental Health Institute (NMHI), University of Alberta ⁴California Institute of Technology (Caltech). Correspondence to: Bahareh Tolooshams <btolooshams@ualberta.ca>.

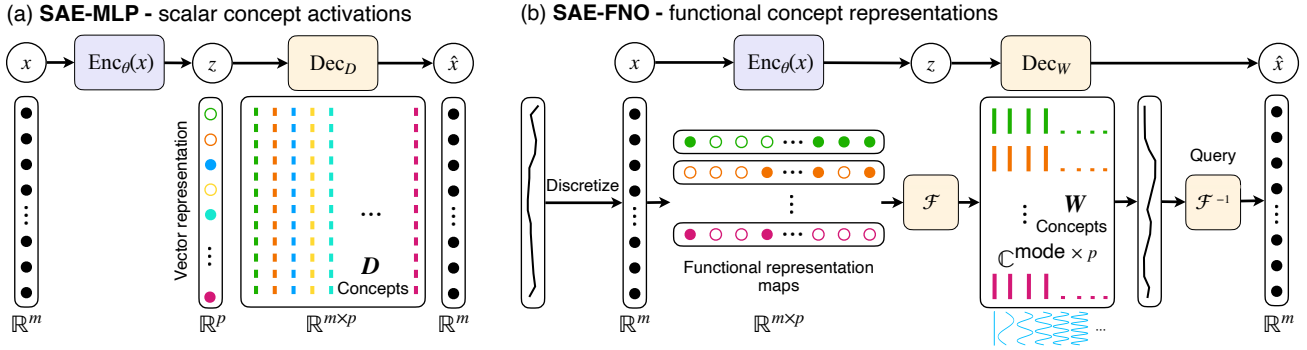


Figure 1. **Sparse Autoencoder Neural Operator (SAE-NO)**. (a) Conventional SAEs (SAE-MLP) parameterize concepts (D) in the Euclidean domain, assigning each concept a scalar activation indicating presence and strength. (b) SAE-FNOs use functional concept parameterization via Fourier integral operators, encoding both *concept sparsity* and *domain sparsity* to capture how and where concepts are expressed. SAE-FNO treats inputs as samples from an underlying continuous function, learns concepts in the Fourier domain, and supports querying of representations, reconstructions, and concepts at varying resolutions.

These properties introduce an inductive bias that can limit the ability of SAEs to learn generalized or localized concepts, or to be applied to data and activations across varying scales. In particular, scalar concept activations, especially when the underlying data exhibit spatial or temporal structure, cannot capture how a concept is expressed, where it manifests locally, in what orientation, or what structural properties of the input domain it encodes. Such capabilities are essential in scientific modelling, computer vision, and in analyzing model activations or physical data that exhibit locality or symmetric structure. While concept feature maps can be introduced through a convolutional parameterization of SAEs (which we introduce as SAE-CNNs), such models remain tied to a fixed resolution and inherit inductive biases imposed by parameterization in the input domain.

This is in contrast with class of deep learning architectures known as neural operators (NO) (Li et al., 2021), which extends beyond Euclidean spaces and learns mappings between infinite-dimensional function spaces. Neural operators are central to data-driven scientific modelling (Azzadenesheli et al., 2024), particularly for solving partial differential equations (PDEs), can generalize across discretizations, and have recently been applied in neuroscience to capture brain representations (Ghafourpour et al., 2025). While their predictive power is well established across applications (Li et al., 2024; Jatyani et al., 2025), their representational properties and capability for concept learning and mechanistic interpretability remain largely unknown.

Our contributions. We focus on extracting concepts from vision data, where local and spatial structure is inherent and where sparse autoencoders should capture such structure across both spatial locations and scales. We introduce sparse autoencoder neural operators (SAE-NOs), a new class of SAEs that operate directly in infinite-dimensional function spaces. We generalize the LRH to a functional representation hypothesis (FRH), enabling the learning and extraction

of concepts in function spaces. Building on FRH, we instantiate SAE-NOs in the form of sparse autoencoder Fourier neural operators (SAE-FNOs).

With SAE-FNO, we introduce a principled tool for mechanistic interpretability (Nanda et al., 2023) in models and data with inherent locality, continuity, or spatial structure. Our results show that when such structure is essential to the underlying concepts, conventional SAEs fail to recover meaningful and expressive representations, while SAE-FNOs effectively capture and exploit these properties.

SAE-FNO parameterizes concepts as integral operators in the Fourier domain. We demonstrate that SAEs impose an inductive bias on the characteristics of learned concepts that depends critically on the domain in which the concepts are *parameterized*. To our knowledge, a systematic study of how concept parameterization shapes the inductive bias of SAEs has not been explored in prior work.

SAE-NOs replace scalar activations with feature-map representations, introducing *domain sparsity* alongside *concept sparsity* to encode *where* and *how* concepts are expressed. This offers structured representations that capture both concept presence and data structure. More precisely, concept sparsity acts as group sparsity (selecting active channels), while domain sparsity is intra-group spatial sparsity. While SAE-CNNs can exhibit a similar abstraction at a fixed resolution, they do not inherit the same benefits as SAE-FNOs in terms of generalization, efficiency of concept utilization, and stability across varying resolutions and sparsity levels.

We visualize the concepts in SAE-FNO and SAE-MLP and show that SAE-FNO exhibits superior expressivity, requiring fewer concepts. SAE-FNO learns concepts that are globally shared across the data population and are reused in different ways through the structure of their feature-map representations. As a result, SAE-FNO achieves significantly higher efficiency in concept utilization.

Compared to SAE-MLP and SAE-CNN, we show that SAE-FNO learns concepts with fundamentally different characteristics. In particular, SAE-FNO generalizes across resolutions, and its learned concepts are stable and robust to the choice of sparsity level and to distribution shifts. While many SAE variants exhibit an inductive bias toward learning approximately orthogonal concepts due to their shallow encoders, SAE-FNOs can learn concepts spanning a broader range of correlations even in the presence of this bias.

We introduce *lifting* into SAEs for concept extraction, mapping inputs to a higher-dimensional space where concept learning is performed. As a core component of neural operators, lifting increases expressivity and improves optimization. We show that lifting acts as a preconditioner that accelerates recovery and filters noise, enabling the learning of smoother and more robust concepts.

2. Preliminaries and Related Works

The sparse linear generative model (Definition 2.1), also known as sparse coding (Olshausen & Field, 1996), has a rich history in statistics and in compressed sensing (Donoho, 2006; Candès et al., 2006). Representing data \mathbf{x} under a *sparse generative model* involves learning a dictionary \mathbf{D}^* to infer a sparse code \mathbf{z} . We focus on the case where \mathbf{D}^* is unknown (a.k.a. *dictionary learning*) (Agarwal et al., 2016) and refer to it as *sparse concept/model recovery*, formulated as a bilevel problem (Definition 2.2) (Tolooshams, 2023).

Definition 2.1 (Sparse Generative Models). A data sample $\mathbf{x} \in \mathbb{R}^m$ is said to follow a sparse generative model if there exists a sparse code $\mathbf{z} \in \mathbb{R}^p$ (with $\text{supp}(\mathbf{z}) \leq k \ll p$) and an overcomplete dictionary $\mathbf{D}^* \in \mathbb{R}^{m \times p}$ (with $p \gg m$) that model the data as $\mathbf{x} = \mathbf{D}^* \mathbf{z}$ in the noiseless setting.

Definition 2.2 (Sparse Concept Recovery). Under the sparse generative model (Definition 2.1), the goal of sparse concept recovery is to estimate the underlying dictionary \mathbf{D}^* by solving the following problem:

$$\begin{aligned} \text{(outer)} \quad & \min_{\mathbf{D} \in \mathcal{D}} \frac{1}{2} \|\mathbf{x} - \mathbf{D}\mathbf{z}\|_2^2 + \lambda \mathcal{R}(\mathbf{z}) \\ \text{s.t. (inner)} \quad & \mathbf{z} = \text{Enc}_\theta(\mathbf{x}) = \arg \min_{\mathbf{v} \in \mathbb{R}^p} \mathcal{L}(\mathbf{x}, \mathbf{v}, \theta), \end{aligned} \quad (1)$$

where Enc_θ is a forward map encoder from data \mathbf{x} to latent code \mathbf{z} , defined as the minimizer of the inner loss $\mathcal{L}(\mathbf{x}, \mathbf{v}, \theta)$. The outer-level optimizes \mathbf{D} , and concept/model recovery is *successful* when the learned concept \mathbf{D} approximates the true underlying dictionary \mathbf{D}^* .

The connection between bilevel optimization and neural networks is well established through SAEs (Malézieux et al., 2022; Tolooshams & Ba, 2022). The inner and outer levels in Definition 2.2 mirror the encoder–decoder structure of a neural network, where the encoder Enc_θ maps data \mathbf{x} to sparse codes \mathbf{z} , and the decoder reconstructs \mathbf{x} via $\mathbf{D}\mathbf{z}$ using learned concepts \mathbf{D} (see Definition 2.3).

Definition 2.3 (Sparse Autoencoders for Concept Recovery). The goal of concept recovery with SAEs is to infer a sparse code $\mathbf{z} \in \mathbb{R}^p$, representing the data $\mathbf{x} \in \mathbb{R}^m$, with a linear combination of a dictionary of concepts \mathbf{D} : (encoder) $\mathbf{z} = \text{Enc}_\theta(\mathbf{x})$, (decoder) $\hat{\mathbf{x}} = \text{Dec}(\mathbf{z}) = \mathbf{D}\mathbf{z}$, where θ denotes the set of encoder parameters. Model recovery refers to learning the concepts \mathbf{D} .

The mechanistic interpretability community is interested in shallow autoencoders as $\text{Enc}(\mathbf{x}) = \mathcal{S}(\mathbf{W}^\top \mathbf{x} + \mathbf{b})$. For mechanistic interpretability, the key distinguishing factor between SAEs is how they design the nonlinear activation (projection) \mathcal{S} to be ReLU (Huben et al., 2023), TopK (Makhzani & Frey, 2014), SpaDE (Hindupur et al., 2025), JumpReLU (Rajamanoharan et al., 2024), Batch-TopK (Bussmann et al.), and MPSAE (Costa et al., 2025).

To extend SAEs to function spaces, we briefly review neural operators (Kovachki et al., 2023), which learn mappings between infinite-dimensional function spaces rather than finite-dimensional Euclidean spaces. Neural operators consist of three components: lifting, kernel integration, and projection (see Appendix). Lifting maps data to a higher-dimensional channel space where learning occurs, followed by projection back to a lower-dimensional space, and improves the optimization of SAEs.

Fourier Neural Operator (FNO) (Li et al., 2021) models the kernel integral operator (Definition A.2) with a convolution operator parameterized in Fourier space (Definition A.3, Definition A.4). The convolution operator parameterizes the kernel $\kappa(x, y) = \kappa(x - y)$ as a complex function $\kappa : D \rightarrow \mathbb{C}^{d_w \times d_v}$. FNO is used with truncated frequency modes in practice, shown to improve performance and lower sensitivity to decreasing the discretization sampling.

3. Sparse Autoencoder Neural Operators

We extend SAEs, typically implemented with MLP-based encoders (SAE-MLPs), to neural operators to enable concept recovery in function spaces. While standard SAEs represent each concept with a scalar activation indicating its presence and strength, we instead learn global feature-map representations whose energy corresponds to the degree to which a concept is utilized. Importantly, the representations encode both localized and global structure, capturing *how* each concept contributes to representing the data (Figure 1).

To introduce SAE-NOs, we define a sparse functional generative model of data to formalize the functional representation hypothesis (FRH) (Definition 3.1) and formulate its corresponding optimization problem for concept recovery in function spaces (Definition 3.2).

Definition 3.1 (Functional Representation Hypothesis (FRH)). Consider a linear operator $\mathcal{G}_{\mathbf{D}^*} : \mathcal{Z} \rightarrow \mathcal{X}$ in function spaces, where \mathcal{Z} and \mathcal{X} are Banach spaces of functions

defined on bounded domains $D_z \subset \mathbb{R}^p$ and $D_x \subset \mathbb{R}^m$, respectively. The data sample $\mathbf{x} \in \mathcal{X}$ is said to follow a sparse functional generative model or the functional representation hypothesis (FRH) if there exists a sparse latent representation \mathbf{z} drawn from the support \mathcal{Z} of a probability measure μ , where $\mathbf{x} = \mathcal{G}_{D^*}(\mathbf{z})$.

Definition 3.2 (Sparse Functional Concept Recovery). Under the sparse functional generative model (Definition 3.1), the goal of sparse concept recovery in function spaces is to estimate the underlying operator \mathcal{G}_{D^*} by solving the following bilevel optimization problem:

$$\begin{aligned} \min_{D \in \mathcal{D}} \quad & \mathbb{E}_{z \sim \mu} \|\mathcal{G}_{D^*}(z) - \mathcal{G}_D(\hat{z})\|_{\mathcal{X}}^2 \\ \text{s.t.} \quad & \hat{z} = \arg \min_v \mathbb{E}_{z \sim \mu} \|v - \mathcal{H}_\theta(\mathcal{G}_{D^*}(z))\|_{\mathcal{Z}}^2, \end{aligned} \quad (2)$$

where the operator $\mathcal{H}_\theta : \mathcal{X} \rightarrow \mathcal{Z}$ aims to approximate the inverse of \mathcal{G}_{D^*} . Model recovery is successful when the learned concepts D in \mathcal{G}_D closely approximate D^* in \mathcal{G}_{D^*} .

To recover concepts, we formalize an SAE-NO (Definition 3.3) with an encoder approximating the inverse generative operator and a decoder that captures the underlying operator and its learnable concepts.

Definition 3.3 (Sparse Autoencoder Neural Operators (SAE-NOs) for Concept Recovery). The goal of model recovery with SAE-NO in function spaces is to infer a sparse representation \mathbf{z} as a sample from the function space \mathcal{Z} , representing the data sample from the function space \mathcal{X} via \mathcal{G}_D : (encoder) $\mathbf{z} = \text{Enc}_\theta(\mathbf{x})$, (decoder) $\hat{\mathbf{x}} = \text{Dec}_D(\mathbf{z})$, where Enc_θ is the encoder operator relating to \mathcal{H}_θ , and model recovery involves estimating the concepts D parameterized within Dec_D .

We consider a Fourier parameterization and define SAE Fourier Neural Operators (SAE-FNOs) as $\mathcal{G}_D(\mathbf{z}) := \mathcal{F}^{-1}(\sum_{c=1}^C \mathbf{W}_c \cdot (\mathcal{F}\mathbf{z}_c))$ where $\mathbf{W}_c = \mathcal{F}D_c$ denotes the Fourier transform of the convolution kernel D_c . SAE-NO is fundamentally different from all other SAEs to date; all SAEs parameterize the concepts in the same domain as the encoder input, mapping the representation via $D\mathbf{z}$ to the reconstruction. SAE-NO, on the other hand, parameterize both encoding and decoding concepts as an integral kernel operator parameterized in Fourier space. We show that this Fourier and functional parameterization plays a critical role in shaping the characterization and generalization of the learned concepts. Owing to the duality between convolution in the spatial domain and multiplication in the Fourier domain, inference in SAE-FNOs can be viewed as recovering concepts under a sparse convolutional generative model (Definition A.1), implemented as a sum of convolutions between \mathbf{z} and D . While SAE-FNO is general and can be applied to SAEs with different activation functions (e.g., ReLU), we introduce two distinct notions of sparsity for SAE-FNO: *concept sparsity* and *domain sparsity*.

Concept sparsity extends standard SAEs by enforcing that only a few concepts explain each data example, while domain sparsity captures the activation pattern within each concept’s feature map. As a result, concept sparsity induces *group sparsity* across feature maps, whereas domain sparsity enforces element-wise sparsity within each map. Intuitively, concept sparsity determines *which* concepts are active, while domain sparsity determines *where* they are expressed in the input domain. We show that this sparsity parameterization enables SAE-FNO to learn globally shared yet locally expressed concepts that are robust to changes in sparsity level. This enables SAE-FNO to represent datasets more compactly, using a smaller number of learned concepts.

For TopK as the activation function, SAE-FNO implements the following:

$$\begin{aligned} \min_{W \in \mathcal{W}} \quad & \frac{1}{2} \|\mathbf{x} - \mathcal{F}^{-1}(\mathbf{W} \cdot \mathcal{F}\mathbf{z} + \mathbf{b}_{\text{pre}})\|_2^2 \\ \text{s.t.} \quad & \mathbf{v} = (\mathcal{F}^{-1}(\mathbf{E} \cdot (\mathcal{F}\mathbf{x} - \mathbf{b}_{\text{pre}})) + \mathbf{b}_{\text{enc}}) \\ \text{(concept sparsity)} \quad & \mathbf{a} = \text{TopK}([\|\mathbf{v}_1\|_2, \dots, \|\mathbf{v}_C\|_2]^\top) \\ & \mathbf{v} = \mathbf{1}_a \cdot \mathbf{v} \\ \text{(domain-sparsity)} \quad & \mathbf{z}_i = \text{TopK}(\mathbf{v}_i), \text{ for } i, \text{ where } \|\mathbf{v}_i\|_2 > 0 \end{aligned} \quad (3)$$

We further extend this approach to concept recovery in lifted spaces (Definition 3.4), incorporating *lifting* and *projection* modules that are crucial components of neural operators.

Definition 3.4 (Lifted SAE-NO for Concept Recovery). The goal of model recovery with lifted SAE-NO (L-SAE-NO) in function spaces is to infer a sparse representation \mathbf{z} as a sample from the function space \mathcal{Z} , representing the data from \mathcal{X} via the operator Dec_{D_L} :

$$\begin{aligned} \text{(lifting and encoder)} \quad & \mathbf{z} = \text{Enc}_\theta(\mathbf{y}), \quad \mathbf{y} = \mathbf{L}\mathbf{x} \\ \text{(decoder and projecting)} \quad & \hat{\mathbf{x}} = \mathbf{P}\hat{\mathbf{y}}, \quad \hat{\mathbf{y}} = \text{Dec}_{D_L}(\mathbf{z}), \end{aligned} \quad (4)$$

where Enc_θ encodes the lifted data \mathbf{y} , and concept recovery is done via the learned lifted concepts D_L .

Proposition 3.5 shows that gradient dynamics of Fourier concepts \mathbf{W} in L-SAE-FNO can be represented as concepts in the original and unlifted space as D where the lifting acts as a preconditioner, which if designed/learned properly can accelerate learning by inducing a more isotropic update. We show in Proposition C.8 that the dynamics of a L-SAE-FNO can be reduced to SAE-FNO when the lifting and projection are tied ($\mathbf{P} = \mathbf{L}^\top$) and the lifting operator is orthogonal ($\mathbf{L}^\top \mathbf{L} = \mathbf{I}$). This highlights that recovery of lifted concepts in relation to the original domain is possible. These results also hold for SAE-MLP and SAE-CNN (see Appendix).

Proposition 3.5 (Training Dynamics of Lifted SAE-FNO). *The training dynamics of the Lifted-SAE-FNO (L-SAE-FNO)’s frequency domain weights $\mathbf{W}_{L,c}^{(k+1)} = \mathbf{W}_{L,c}^{(k)} +$*

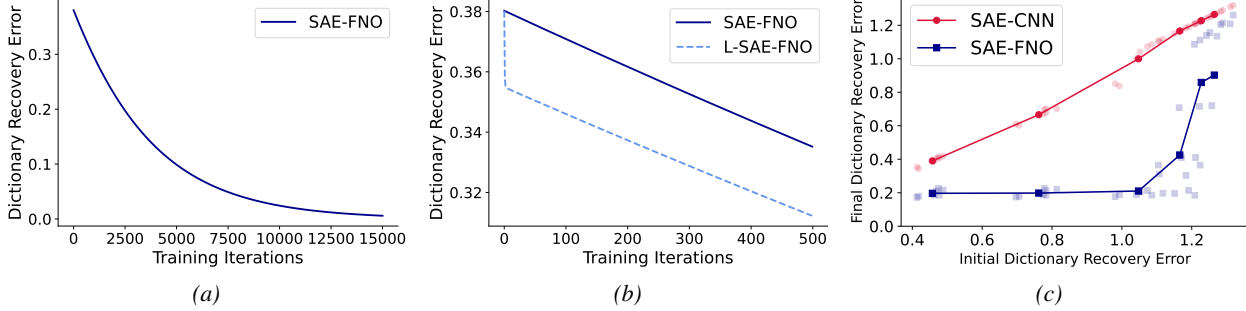


Figure 2. Concept Recovery Examined Under Known Generative Model. (a) SAE-FNOs can recover underlying concepts. The dictionary (concept) recovery error converges to zero as a function of training iterations. (b) Lifting the SAE onto a high-dimensional space for concept learning acts as a preconditioner and accelerates recovery. (c) SAE-FNO is superior to SAE-CNN in recovering smooth concepts. Each dot represents one training scenario with x-axis as the initialized concept error and y-axis as the final trained concept error.

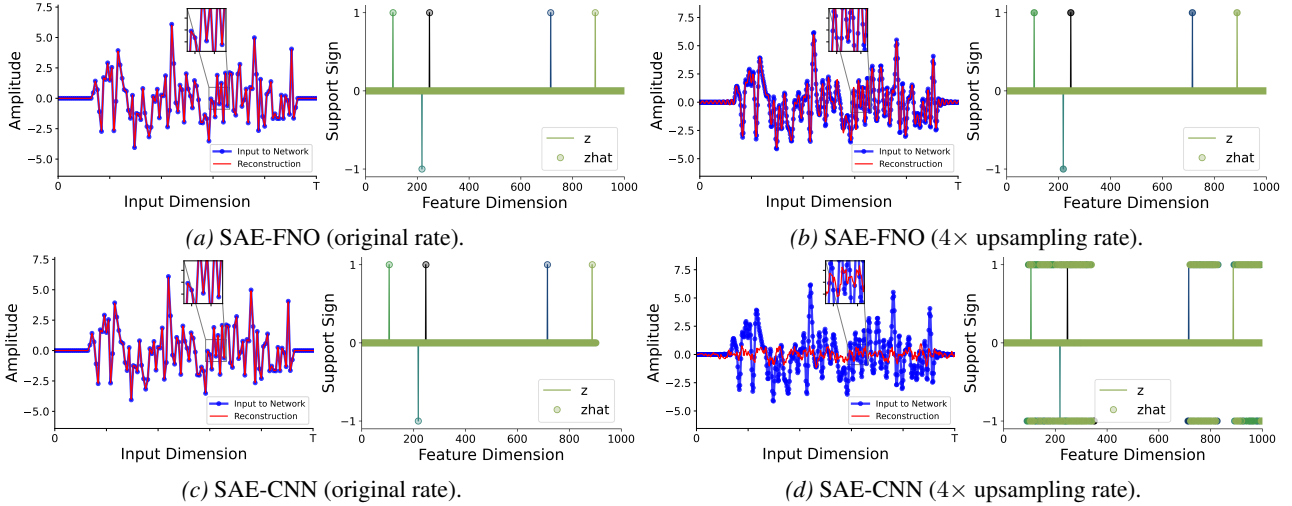


Figure 3. Discretization Generalization of SAE-FNO. The underlying data structure has five convolutional concepts along with a 5-sparse code (i.e., 1-sparse representation for each concept). Each subplot shows (left) the input data and its reconstruction, and (right) the support sign (active sparse codes). (a-b) SAE-FNO can successfully infer the underlying sparse representations and reconstruct the data at the original as well as an increased rate. (c-d) While SAE-CNN can reconstruct the data and infer the sparse representation at the original rate, it fails to represent the data at a resolution different from the one trained at (see also Figure 11).

$\frac{\eta_L}{\sqrt{M}} \mathcal{F}(\mathbf{L}(\mathbf{x} - \hat{\mathbf{x}}^{(k)})) \odot \mathcal{F}(\mathbf{z}_{c,k})$, with lifting operator \mathbf{L} and projection \mathbf{P} , has an effective update in the original space, expressed as: $\mathbf{D}_c^{(k+1)} = \mathbf{D}_c^{(k)} + \frac{\eta_L}{M} ((\mathbf{L}^\top \mathbf{L})(\mathbf{x} - \hat{\mathbf{x}}^{(k)})) \star \mathbf{z}_{c,t}$, where $\mathbf{L}^\top \mathbf{L}$ acts as a preconditioner, potentially. If the architectures satisfy the architectural inference equivalence condition (Proposition C.8), then the dynamics is equivalent to that of an SAE-FNO: $\mathbf{D}_c^{(k+1)} = \mathbf{D}_c^{(k)} + \frac{\eta}{M} \left(\mathbf{x} - \frac{1}{\sqrt{M}} \mathcal{F}^{-1} \left(\sum_{i=1}^C \mathcal{F}(\mathbf{D}_i^{(k)}) \odot \mathcal{F}(\mathbf{z}_{i,k}) \right) \right) \star \mathbf{z}_{c,k}$.

4. Results

In model interpretability, SAEs are commonly used in two settings. One approach trains SAEs on internal model representations to identify latent concepts (Huben et al., 2023), but this requires additional post-processing to map internal features to human-interpretable attributes, introducing

practical complexity. Alternatively, recent work trains SAEs directly on samples from the model’s output distribution, operating on human-interpretable signals rather than internal activations (Bohacek et al., 2025; Jiang et al., 2025). This paradigm is particularly attractive for generative models, as it enables direct analysis of generated data and learned concepts without explicit alignment steps. We adopt this second approach and train SAE-FNOs directly on data with local, temporal, and spatial structure, comparing them to standard SAEs to enable immediate interpretation of learned concepts in the data domain.

Concept Recovery Under Known Generative Model.

We first characterize SAE-FNO under a known ground-truth generative model. We instantiate the model with an unrolled encoder (Tolooshams & Ba, 2022) (see Appendix for details). As shown in Figure 2a, SAE-FNO is successful in identifying the underlying generative model and learning the ground-truth concepts. We further analyze concept re-

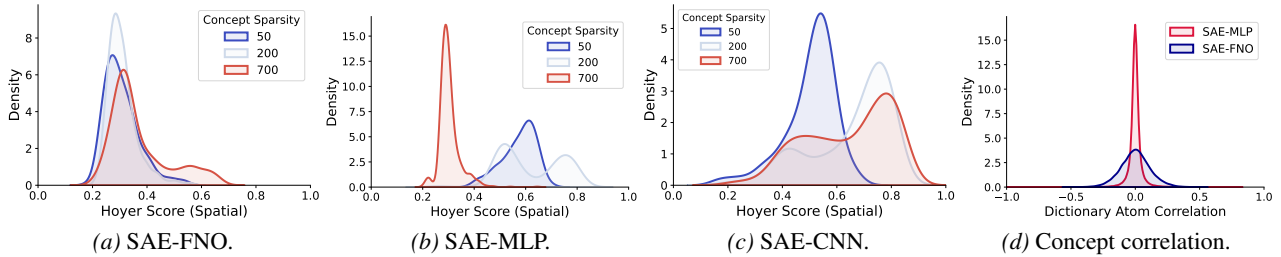


Figure 4. SAE-NO concept characterization and stability. We use the Hoyer score to characterize the locality and sparsity of the learned concepts, and examine the concept correlations (a) SAE-FNO shows stable concept characteristics across different concept sparsity levels. (b) In contrast, the characteristics of concepts learned by SAE change drastically as the sparsity level varies, indicating an undesirable sensitivity of concept properties to this choice. (c) Comparison of concept correlations for SAE-FNO and SAE-CNN: SAE-FNO exhibits a broader range of correlations, even in the presence of a shallow, orthogonality-inducing inductive bias.

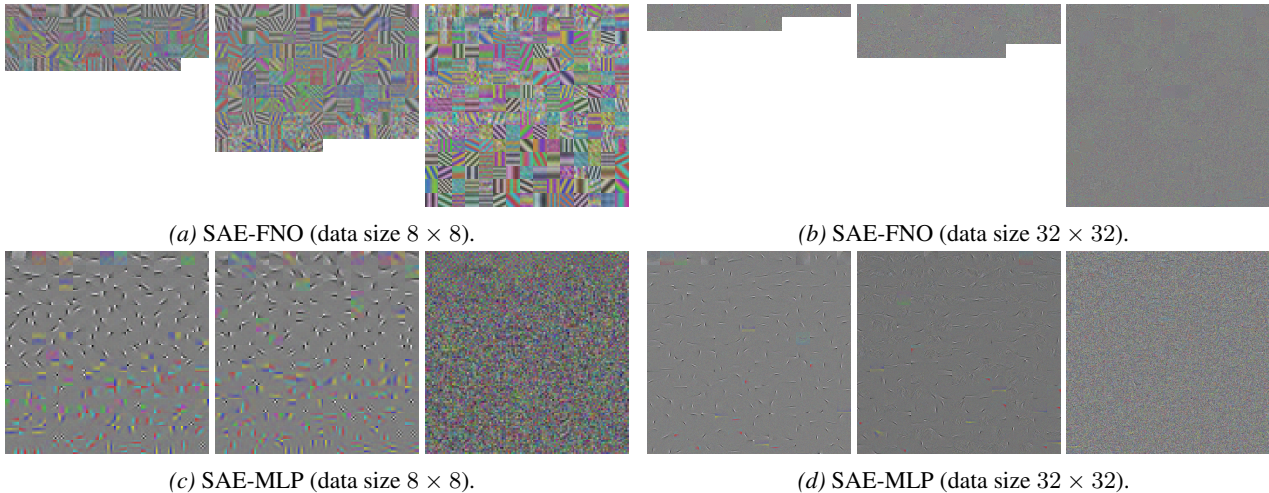


Figure 5. Visualization of used concepts, across the full population, learned by SAE-FNO and SAE-MLP. From left to right, the concept sparsity is set to 25, 50, and 200. (a–b) SAE-FNO exhibits stable concept characteristics across varying levels of concept sparsity, enabled by domain sparsity and the ability to adapt to different input domain sizes. As concept sparsity decreases, a larger number of concepts are activated across the dataset. For localized image patches (8×8), SAE-FNO learns sinusoidal patterns at varying frequencies, while for larger inputs (32×32), it learns localized frequency patterns such as edge detectors. (c–d) In contrast, the characteristics of concepts learned by SAE-MLP change drastically as concept sparsity increases, leading to a loss of interpretable structure. Moreover, SAE-MLP lacks the capacity to capture local spatial structure in the data. Hence, an important observation is that particularly, when data domain gets larger, the effective number of learned concepts in SAE-FNO is substantially smaller than in SAE-MLP, indicating the superior expressivity of SAE-FNO, particularly for inputs with large domains and localized structure.

covery in the lifted space, and found: i) underlying concepts can be recovered in the lifted space; ii) lifting can act as a preconditioner (Proposition 3.5), accelerating recovery (Figure 2b) by reducing dictionary atom correlation, promoting a more isotropic loss landscape (Figure 10); ; iii) when lifting and projection are tied and orthogonal, the architectural inference (Proposition C.8) and training dynamics (Proposition 3.5) of L-SAE-NO reduces to SAE-NO.

SAE-NO Discretization Capability. Conventional SAEs operate on fixed-grid data in Euclidean spaces such as \mathbb{R}^n , with representations tied to a specific resolution. In contrast, the functional parameterization of SAE-FNOs inherits key advantages of neural operators, enabling analysis and inference across discretization levels. We demonstrate this capability under a known generative model (Figure 3), where

SAE-FNO, unlike SAE-CNN, generalizes to data at higher resolutions than those seen during training. We further validate this property on MNIST (Figure 11): an SAE-NO with $p = 1000$ concepts trained at 28×28 continues to represent data accurately up to 112×112 , while the reconstruction error of a standard SAE increases sharply beyond the training resolution. This discretization generalization persists across different frequency truncations.

SAE-NO Concept Stability and Correlation A defining characteristic of SAE-NOs that distinguishes them from existing SAEs lies in their *concept parameterization*. In particular, SAE-FNOs parameterize concepts in the Fourier domain. We characterize the learned concepts using the Hoyer score, a normalized measure for sparsity in $[0, 1]$, where 1 indicates a fully sparse concept and 0 indicates a

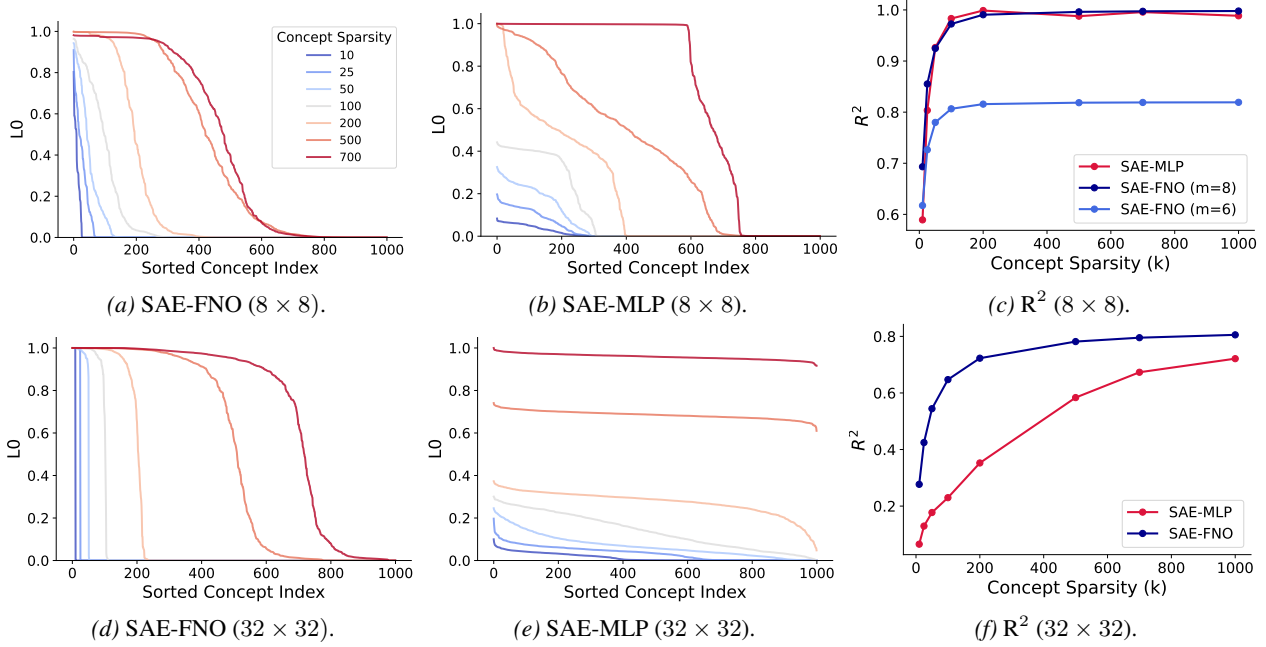


Figure 6. Concept utilization and expressivity by SAE-FNO and SAE-MLP. (a,b,d,e) The ℓ_0 code statistics (y-axis) across the data population are plotted against concept indices, sorted by decreasing ℓ_0 utilization (x-axis). (c,f) Goodness-of-fit (R^2). SAE-FNO shows a much sharper decrease in concept utilization as a function of number of concepts compared to SAE-MLP. The area under the curve (concept utilization) quantifies the number of learned concepts required to characterize the data. The flatter curve for SAE-MLP suggests that as data domain grows, SAE-MLPs require a much larger number of concepts to achieve the same representation capability as SAE-FNO. This implies that the concepts learned by SAE-FNO are more generalizable and used more globally and efficiently across the dataset. The R^2 results demonstrate the limited capacity of SAE-MLP to capture the underlying local structure of the data population.

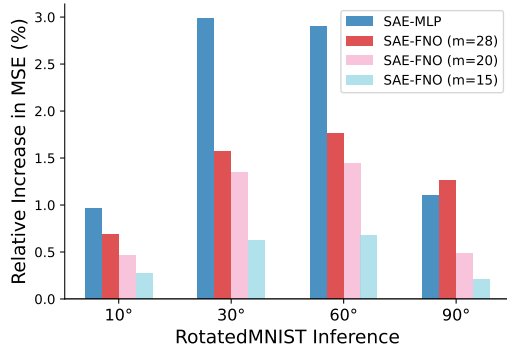


Figure 7. Generalization of SAE concepts under data distribution shift. Under a distribution shift induced by data rotation, the reconstruction error of SAE-MLP increases sharply relative to in-distribution performance. In contrast, SAE-FNO learns more generalizable concepts, leading to a substantially smaller increase in reconstruction error on out-of-distribution samples. This behavior is consistent across a wide range of Fourier modes (15, 20, and 28) used in the architecture.

fully dense concept. We compute the score for each concept individually. For a flattened representation $v_c \in \mathbb{R}^N$ of the c -th concept, the Hoyer score is given by:

$$\text{Hoyer}(v_c) = \frac{\sqrt{N} - \frac{\|v_c\|_1}{\|v_c\|_2}}{\sqrt{N} - 1} \quad (5)$$

We report the distribution of these scores over all p concepts

to characterize the sparsity of the learned dictionary.

As shown in Figure 4a, this parameterization offers concepts whose characteristics, quantified by the Hoyer score, remain stable and robust across different choices of sparsity level in the representation. In contrast, the characteristics of concepts learned by standard SAEs (Figure 4b) vary substantially as the sparsity level changes. We emphasize that such stability is a crucial and desirable property in practical applications: when learned concepts are highly sensitive to the choice of sparsity level, it becomes unclear which concepts can be reliably interpreted or trusted by the user.

Another important property of SAE-NOs is their flexibility in learning *correlated* concepts. This contrasts with the inductive bias of shallow SAEs, which tend to learn approximately orthogonal concepts (Costa et al., 2025). While recent work has begun to move beyond strict orthogonality, it remains desirable to develop SAEs that can learn non-orthogonal concepts even in the presence of orthogonality-inducing biases. Figure 4d illustrates this capability for SAE-FNOs compared to CNN-based counterparts. The histogram of pairwise concept correlations for SAE-FNOs exhibits a broader distribution, whereas SAE-CNNs show a sharply peaked distribution centered near zero. This increased flexibility stems from the functional parameterization of SAE-FNOs, which associates each concept with a

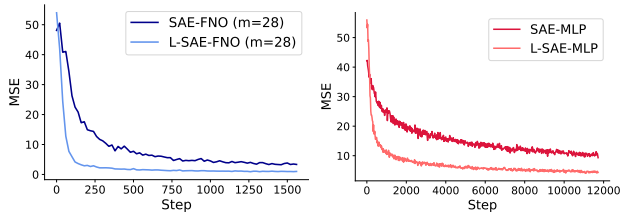


Figure 8. Lifting accelerates and improves performance. Lifting acts as a preconditioner introducing an implicit acceleration to learning. In real-world setting, this can result in better fit of data by reducing the impact of noise on learned concepts. The impact of lifting also extends to conventional SAEs (left) SAE-FNO vs. Lifted SAE-FNO. (right) SAE vs. Lifted SAE.

feature-map representation. As a result, SAE-FNOs can learn concepts with similar overall code energy that differ in how and where they are expressed across the input domain, for example by appearing in different local regions.

Concept Visualization and Utilization. We visualize the learned concepts on natural images and examine their utilization across the data population (see Appendix for detailed experimental setup). We particularly show how conventional SAEs fail when the underlying model/data exhibit spatially local structure, which cannot be efficiently extracted by SAE-MLPs. Figure 5 shows that the SAE-FNO learns sinusoidal filters for local patches and localized frequency patterns for larger images. While such concept characteristic of SAE-FNO is stable against the concept sparsity level, concepts learned by SAE-MLP change drastically as concept sparsity increases, losing interpretable structure.

This qualitative difference directly explains the efficiency observed in Figure 6, where we examine concept utilization across the population. SAE-FNO exhibits a significantly sharper decrease in concept usage across the data population, implying that a smaller, compact set of these structured concepts is sufficient to characterize the dataset. In contrast, SAE-MLP shows a much flatter distribution, requiring a significantly larger number of active concepts. While both models may achieve comparable reconstruction (R^2) on small domains (patches), SAE-FNO outperforms SAE-MLP on larger image domain, due to the need to extract local structures for generalization. Additionally, we argue that the primary advantage of SAE-FNO lies in the characteristics of the learned concepts and their interpretability. Consequently, our analysis focuses on these properties, such as stability, resolution invariance, and structure, and we prioritize these over reconstruction metrics.

Lifting Accelerated Learning and Improved Performance. An additional contribution of our work is the ability to *lift* an SAE into a latent space and perform concept and sparse representation learning in this lifted domain. Complementing our earlier lifted results, we now shows that, beyond faster convergence, lifting provides two key benefits (Figure 8): (i) the acceleration effect extends beyond

operator-based SAEs and applies to non-operator SAEs, and (ii) lifting improves concept learning, leading to lower reconstruction error. This gain can be interpreted through mechanisms akin to the implicit regularization of gradient descent in deep models (Neysshabur, 2017; Arora et al., 2019). From a concept learning perspective, lifting shifts stochasticity and noise to the lifted space, while linear projection back to the original domain induces a smoothing effect that facilitates the extraction of more robust, higher signal-to-noise concepts.

Concept Generalization Under Distribution Shift. Finally, we show that SAE-FNO learns more generalizable concepts than SAE-MLP under a distribution shift induced by image rotation (Figure 7). While standard SAEs exhibit a substantial increase in reconstruction error, SAE-NOs show a much smaller relative increase in mean squared error, indicating more stable and representative concepts. We note that this experiment provides preliminary insight into concept generalization under distribution shift; a comprehensive ablation study of out-of-distribution generalization is left for future work.

5. Conclusion

We introduced sparse autoencoder neural operators (SAE-NOs), a framework generalizing sparse representation learning to infinite-dimensional function spaces. By parameterizing concepts in the Fourier domain via SAE-FNO, we move beyond scalar activations to feature-map representations that explicitly encode where and how concepts are expressed through domain sparsity. We demonstrated that this functional parameterization fundamentally enhances concept learning: SAE-NOs exhibit resolution invariance, robust recovery under distribution shifts, and stability in learned concept characteristics across varying sparsity levels. Our findings highlight parameterization as crucial in shaping learned representations. Moreover, we showed that the lifting mechanism acts as a preconditioner, accelerating recovery and improving robustness to noise, enabling high-SNR concept learning.

In this work, we focus on vision datasets with local structure and perform concept learning in a controlled setting to better characterize this new model. While our primary goal is to analyze the concepts learned by SAE-NOs and demonstrate that functional parameterization fundamentally improves concept learning in sparse autoencoders, several limitations remain. In particular, our empirical evaluation is restricted to controlled vision experiments and moderate-scale real data; extending SAE-NOs to large-scale, high-dimensional settings, such as foundation model activations or complex scientific simulations, requires further investigation.

Impact Statement

This work advances the field of machine learning by introducing a new framework for representation learning and interpretability based on sparse autoencoder neural operators (SAE-NO). By extending sparse autoencoders to functional and multi-resolution settings, our approach enables more stable, generalizable, and interpretable concept representations, with potential benefits for scientific modelling and mechanistic interpretability in general.

The methods proposed here are intended for understanding and characterizing learned representations rather than for deployment in high-stakes decision-making systems. Hence, we do not anticipate immediate negative societal impacts. However, as with any interpretability or representation learning tool, insights derived from these models could influence how complex systems are analyzed or trusted. Care should therefore be taken when applying SAEs in sensitive domains, and conclusions should be interpreted in conjunction with domain expertise.

Overall, this work aims to contribute foundational insights into representation learning and interpretability. We do not identify any foreseeable ethical concerns specific to this contribution.

References

- Ablin, P., Moreau, T., Massias, M., and Gramfort, A. Learning step sizes for unfolded sparse coding. In *Proceedings of Advances in Neural Information Processing Systems*, volume 32, pp. 1–11, 2019.
- Agarwal, A., Anandkumar, A., Jain, P., and Netrapalli, P. Learning sparsely used overcomplete dictionaries via alternating minimization. *SIAM Journal on Optimization*, 26(4):2775–2799, 2016.
- Aharon, M., Elad, M., and Bruckstein, A. K-svd: An algorithm for designing overcomplete dictionaries for sparse representation. *IEEE Transactions on Signal Processing*, 54(11):4311–4322, 2006.
- Arora, S., Ge, R., Ma, T., and Moitra, A. Simple, efficient, and neural algorithms for sparse coding. In Grünwald, P., Hazan, E., and Kale, S. (eds.), *Proceedings of Conference on Learning Theory*, volume 40 of *Proceedings of Machine Learning Research*, pp. 113–149, Paris, France, 03–06 Jul 2015. PMLR.
- Arora, S., Cohen, N., Hu, W., and Luo, Y. Implicit regularization in deep matrix factorization. *Advances in Neural Information Processing Systems*, 32, 2019.
- Azizzadenesheli, K., Kovachki, N., Li, Z., Liu-Schiaffini, M., Kossaifi, J., and Anandkumar, A. Neural operators for accelerating scientific simulations and design. *Nature Reviews Physics*, pp. 1–9, 2024.
- Ba, D. Deeply-sparse signal representations (ds2p). *IEEE Transactions on Signal Processing*, 68:4727–4742, 2020.
- Beck, A. and Teboulle, M. A fast iterative shrinkage-thresholding algorithm for linear inverse problems. *SIAM journal on imaging sciences*, 2(1):183–202, 2009.
- Bengio, Y., Courville, A., and Vincent, P. Representation learning: A review and new perspectives. *IEEE transactions on pattern analysis and machine intelligence*, 35(8): 1798–1828, 2013.
- Bohacek, M., Fel, T., Agrawala, M., and Lubana, E. S. Uncovering conceptual blindspots in generative image models using sparse autoencoders. *arXiv:2506.19708*, 2025.
- Bricken, T., Templeton, A., Batson, J., Chen, B., Jermyn, A., Conerly, T., Turner, N., Anil, C., Denison, C., Askell, A., Lasenby, R., Wu, Y., Kravec, S., Schiefer, N., Maxwell, T., Joseph, N., Hatfield-Dodds, Z., Tamkin, A., Nguyen, K., McLean, B., Burke, J. E., Hume, T., Carter, S., Henighan, T., and Olah, C. Towards monosemanticity: Decomposing language models with dictionary learning. *Transformer Circuits Thread*, 2023a. <https://transformer-circuits.pub/2023/monosemantic-features/index.html>.

- Bricken, T., Templeton, A., Batson, J., Chen, B., Jermyn, A., Conerly, T., Turner, N., Anil, C., Denison, C., Askell, A., et al. Towards monosemanticity: Decomposing language models with dictionary learning. *Transformer Circuits Thread*, 2, 2023b.
- Bussmann, B., Leask, P., and Nanda, N. Batchtopk sparse autoencoders. In *NeurIPS 2024 Workshop on Scientific Methods for Understanding Deep Learning*.
- Bussmann, B., Nabeshima, N., Karvonen, A., and Nanda, N. Learning multi-level features with matryoshka sparse autoencoders. In *Forty-second International Conference on Machine Learning*, 2025. URL <https://openreview.net/forum?id=m25T5rAy43>.
- Candès, E. J., Romberg, J., and Tao, T. Robust uncertainty principles: Exact signal reconstruction from highly incomplete frequency information. *IEEE Transactions on information theory*, 52(2):489–509, 2006.
- Chatterji, N. S. and Bartlett, P. L. Alternating minimization for dictionary learning: Local convergence guarantees. *preprint arXiv:1711.03634*, 2017.
- Chen, S. S., Donoho, D. L., and Saunders, M. A. Atomic decomposition by basis pursuit. *SIAM review*, 43(1): 129–159, 2001.
- Chen, X., Liu, J., Wang, Z., and Yin, W. Theoretical linear convergence of unfolded ista and its practical weights and thresholds. In *Proceedings of Advances in Neural Information Processing Systems*, volume 31, pp. 1–11, 2018.
- Cleary, B., Cong, L., Cheung, A., Lander, E. S., and Regev, A. Efficient generation of transcriptomic profiles by random composite measurements. *Cell*, 171(6):1424–1436.e18, 2017. ISSN 0092-8674.
- Cleary, B., Simonton, B., Bezney, J., Murray, E., Alam, S., Sinha, A., Habibi, E., Marshall, J., Lander, E. S., Chen, F., et al. Compressed sensing for highly efficient imaging transcriptomics. *Nature Biotechnology*, pp. 1–7, 2021.
- Costa, V., Fel, T., Lubana, E. S., Tolooshams, B., and Ba, D. From flat to hierarchical: Extracting sparse representations with matching pursuit. In *Advances in Neural Information Processing Systems*, 2025.
- Daubechies, I., Defrise, M., and De Mol, C. An iterative thresholding algorithm for linear inverse problems with a sparsity constraint. *Communications on Pure and Applied Mathematics*, 57(11):1413–1457, 2004.
- Donoho, D. L. Compressed sensing. *IEEE Transactions on information theory*, 52(4):1289–1306, 2006.
- Doshi-Velez, F. and Kim, B. Towards a rigorous science of interpretable machine learning. *preprint arXiv:1702.08608*, 2017.
- Elad, M. *Sparse and redundant representations: from theory to applications in signal and image processing*. Springer Science & Business Media, 2010.
- Elhage, N., Hume, T., Olsson, C., Schiefer, N., Henighan, T., Kravec, S., Hatfield-Dodds, Z., Lasenby, R., Drain, D., Chen, C., et al. Toy models of superposition. *arXiv:2209.10652*, 2022.
- Fel, T., Boutin, V., Béthune, L., Cadène, R., Moayeri, M., Andéol, L., Chalvidal, M., and Serre, T. A holistic approach to unifying automatic concept extraction and concept importance estimation. *Advances in Neural Information Processing Systems*, 36:54805–54818, 2023.
- Fel, T., Lubana, E. S., Prince, J. S., Kowal, M., Boutin, V., Papadimitriou, I., Wang, B., Wattenberg, M., Ba, D. E., and Konkle, T. Archetypal sae: Adaptive and stable dictionary learning for concept extraction in large vision models. In *Forty-second International Conference on Machine Learning*, 2025.
- Gao, L., la Tour, T. D., Tillman, H., Goh, G., Troll, R., Radford, A., Sutskever, I., Leike, J., and Wu, J. Scaling and evaluating sparse autoencoders. In *The Thirteenth International Conference on Learning Representations*, 2025. URL <https://openreview.net/forum?id=tcsZt9ZNKD>.
- Ghafourpour, L., Duruisseaux*, V., Tolooshams*, B., Wong, P. H., Anastassiou, C. A., and Anandkumar, A. Noble–neural operator with biologically-informed latent embeddings to capture experimental variability in biological neuron models. *arXiv:2506.04536*, 2025.
- Gregor, K. and LeCun, Y. Learning fast approximations of sparse coding. In *Proceedings of international conference on international conference on machine learning*, pp. 399–406, 2010.
- Hershey, J. R., Roux, J. L., and Wenginger, F. Deep unfolding: Model-based inspiration of novel deep architectures. *preprint arXiv:1409.2574*, 2014.
- Hindupur, S. S. R., Lubana, E. S., Fel, T., and Ba, D. E. Projecting assumptions: The duality between sparse autoencoders and concept geometry. In *The Thirty-ninth Annual Conference on Neural Information Processing Systems*, 2025. URL <https://openreview.net/forum?id=SoA8rMxDaF>.
- Huben, R., Cunningham, H., Smith, L. R., Ewart, A., and Sharkey, L. Sparse autoencoders find highly interpretable features in language models. In *The Twelfth International Conference on Learning Representations*, 2023.

- Jatyani, A. S., Wang, J., Wu, Z., Liu-Schiaffini, M., Tolooshams, B., and Anandkumar, A. Unifying subsampling pattern variations for compressed sensing mri with neural operators. *IEEE Conference on Computer Vision and Pattern Recognition (CVPR)*, 2025.
- Jiang, N., Sun, X., Dunlap, L., Smith, L., and Nanda, N. Interpretable embeddings with sparse autoencoders: A data analysis toolkit. *arXiv:2512.10092*, 2025.
- Karvonen, A., Rager, C., Lin, J., Tigges, C., Bloom, J. I., Chanin, D., Lau, Y.-T., Farrell, E., McDougall, C. S., Ayonrinde, K., Till, D., Wearden, M., Conmy, A., Marks, S., and Nanda, N. SAEbench: A comprehensive benchmark for sparse autoencoders in language model interpretability. In *Forty-second International Conference on Machine Learning*, 2025. URL <https://openreview.net/forum?id=qrU3yNfX0d>.
- Kovachki, N., Li, Z., Liu, B., Azzadenesheli, K., Bhattacharya, K., Stuart, A., and Anandkumar, A. Neural operator: Learning maps between function spaces with applications to pdes. *Journal of Machine Learning Research*, 24(89):1–97, 2023.
- Li, Z., Kovachki, N. B., Azzadenesheli, K., liu, B., Bhattacharya, K., Stuart, A., and Anandkumar, A. Fourier neural operator for parametric partial differential equations. In *International Conference on Learning Representations*, 2021. URL <https://openreview.net/forum?id=c8P9NQVtmn0>.
- Li, Z., Kovachki, N., Choy, C., Li, B., Kossaifi, J., Otta, S., Nabian, M. A., Stadler, M., Hundt, C., Azzadenesheli, K., et al. Geometry-informed neural operator for large-scale 3d pdes. *Advances in Neural Information Processing Systems*, 36, 2024.
- Lieberum, T., Rajamanoharan, S., Conmy, A., Smith, L., Sonnerat, N., Varma, V., Kramar, J., Dragan, A., Shah, R., and Nanda, N. Gemma scope: Open sparse autoencoders everywhere all at once on gemma 2. In *The 7th BlackboxNLP Workshop*, 2024. URL <https://openreview.net/forum?id=XkMrWOJhNd>.
- Makhzani, A. and Frey, B. k-sparse autoencoders, 2014. URL <https://arxiv.org/abs/1312.5663>.
- Malézieux, B., Moreau, T., and Kowalski, M. Understanding approximate and unrolled dictionary learning for pattern recovery. In *International Conference on Learning Representations*, 2022.
- Marks, S., Rager, C., Michaud, E. J., Belinkov, Y., Bau, D., and Mueller, A. Sparse feature circuits: Discovering and editing interpretable causal graphs in language models. In *The Thirteenth International Conference on Learning Representations*, 2025. URL <https://openreview.net/forum?id=I4e82CIDxv>.
- Merullo, J., Smith, N. A., Wiegrefe, S., and Elazar, Y. On linear representations and pretraining data frequency in language models. *preprint arXiv:2504.12459*, 2025.
- Monga, V., Li, Y., and Eldar, Y. C. Algorithm unrolling: Interpretable, efficient deep learning for signal and image processing. *IEEE Signal Processing Magazine*, 38(2):18–44, 2021.
- Nanda, N., Chan, L., Lieberum, T., Smith, J., and Steinhart, J. Progress measures for grokking via mechanistic interpretability. In *The Eleventh International Conference on Learning Representations*, 2023. URL <https://openreview.net/forum?id=9XF5bDPmdW>.
- Neyshabur, B. Implicit regularization in deep learning. *preprint arXiv:1709.01953*, 2017.
- Nguyen, T. V., Wong, R. K., and Hegde, C. On the dynamics of gradient descent for autoencoders. In *Proceedings of International Conference on Artificial Intelligence and Statistics*, pp. 2858–2867. PMLR, 2019.
- Olshausen, B. A. and Field, D. J. Emergence of simple-cell receptive field properties by learning a sparse code for natural images. *Nature*, 381(6583):607–609, 1996.
- Papayan, V., Romano, Y., and Elad, M. Convolutional neural networks analyzed via convolutional sparse coding. *Journal of Machine Learning Research*, 18(83):1–52, 2017a.
- Papayan, V., Sulam, J., and Elad, M. Working locally thinking globally: Theoretical guarantees for convolutional sparse coding. *IEEE Transactions on Signal Processing*, 65(21):5687–5701, 2017b.
- Parikh, N. and Boyd, S. Proximal algorithms. *Foundations and Trends in optimization*, 1(3):127–239, 2014.
- Park, K., Choe, Y. J., and Veitch, V. The linear representation hypothesis and the geometry of large language models. In *International Conference on Machine Learning*, pp. 39643–39666. PMLR, 2024.
- Rajamanoharan, S., Lieberum, T., Sonnerat, N., Conmy, A., Varma, V., Kramár, J., and Nanda, N. Jumping ahead: Improving reconstruction fidelity with jumprelu sparse autoencoders. *preprint arXiv:2407.14435*, 2024.
- Rambhatla, S., Li, X., and Haupt, J. Noodl: Provable online dictionary learning and sparse coding. In *Proceedings of International Conference on Learning Representations*, pp. 1–11, 2018.

- Rangamani, A., Mukherjee, A., Basu, A., Arora, A., Ganapathi, T., Chin, S., and Tran, T. D. Sparse coding and autoencoders. In *Proceedings of IEEE International Symposium on Information Theory (ISIT)*, pp. 36–40, 2018.
- Ranzato, M. a., Poultney, C., Chopra, S., and Cun, Y. Efficient learning of sparse representations with an energy-based model. In *Advances in Neural Information Processing Systems*, volume 19. MIT Press, 2007.
- Ranzato, M. a., Boureau, Y.-l., and Cun, Y. Sparse feature learning for deep belief networks. In Platt, J., Koller, D., Singer, Y., and Roweis, S. (eds.), *Proceedings of Advances in Neural Information Processing Systems*, volume 20, 2008.
- Templeton, A., Conerly, T., Marcus, J., Lindsey, J., Bricken, T., Chen, B., Pearce, A., Citro, C., Ameisen, E., Jones, A., Cunningham, H., Turner, N. L., McDougall, C., MacDiarmid, M., Freeman, C. D., Summers, T. R., Rees, E., Batson, J., Jermyn, A., Carter, S., Olah, C., and Henighan, T. Scaling monosemanticity: Extracting interpretable features from claude 3 sonnet. *Transformer Circuits Thread*, 2024. URL <https://transformer-circuits.pub/2024/scaling-monosemanticity/index.html>.
- Tibshirani, R. Regression shrinkage and selection via the lasso. *Journal of the Royal Statistical Society. Series B (Methodological)*, 58(1):267–288, 1996. ISSN 00359246.
- Tolooshams, B. *Deep Learning for Inverse Problems in Engineering and Science*. PhD thesis, Harvard University, 2023.
- Tolooshams, B. and Ba, D. E. Stable and interpretable unrolled dictionary learning. *Transactions on Machine Learning Research*, 2022.
- Tolooshams, B., Song, A., Temereanca, S., and Ba, D. Convolutional dictionary learning based auto-encoders for natural exponential-family distributions. In III, H. D. and Singh, A. (eds.), *Proceedings of the 37th International Conference on Machine Learning*, volume 119 of *Proceedings of Machine Learning Research*, pp. 9493–9503. PMLR, 7 2020.

A. Appendix - Additional Background

Notations We denote scalars as non-bold-lower-case a , vectors as bold-lower-case \mathbf{a} , and matrices as upper-case letters \mathbf{A} .

Sparse model recovery has attracted interest from two representation learning communities: a) *unrolled learning*, using optimization-inspired architectures for learning sparse representation (Ablin et al., 2019; Mal  zieux et al., 2022; Tolooshams & Ba, 2022; Nguyen et al., 2019; Arora et al., 2015; Chen et al., 2018; Rangamani et al., 2018; Tolooshams et al., 2020; Rambhatla et al., 2018); and b) *sparse interpretability* or mechanistic interpretability, employing SAEs to extract concepts from large models (Elhage et al., 2022; Huben et al., 2023; Bricken et al., 2023b; Rajamanoharan et al., 2024; Park et al., 2024; Templeton et al., 2024; Lieberum et al., 2024; Gao et al., 2025; Fel et al., 2025; Marks et al., 2025; Karvonen et al., 2025).

Sparse model recovery The bi-level optimization (Definition 2.2) takes a general form. When the inner level objective $\mathcal{L}(\mathbf{x}, \mathbf{v}, \theta) = \frac{1}{2}\|\mathbf{x} - \mathbf{D}\mathbf{v}\|_2^2 + \mathcal{R}(\mathbf{v})$, this problem is reduced to the classical alternating-minimization dictionary learning (Agarwal et al., 2016; Chatterji & Bartlett, 2017). In this classical form, sparse coding is widely applied in science and engineering; e.g., in signal processing (Elad, 2010), image denoising (Aharon et al., 2006), and extracting interpretable gene modules (Cleary et al., 2017; 2021). When the model parameters \mathbf{D} are known, the problem is reduced to recovering the sparse representation by solving $\min_{\mathbf{z} \in \mathbb{R}^p} \frac{1}{2}\|\mathbf{x} - \mathbf{D}\mathbf{z}\|_2^2 + \lambda\mathcal{R}(\mathbf{z})$, where $\mathcal{R}(\mathbf{z})$ is a sparse regularizer; setting $\mathcal{R}(\mathbf{z}) = \|\mathbf{z}\|_1$, the optimization problem is reduced down to lasso (Tibshirani, 1996), or referred to as basis pursuit (Chen et al., 2001), solving via proximal gradient descent (Parikh & Boyd, 2014) such as iterative shrinkage-thresholding algorithm (ISTA) (Daubechies et al., 2004) and its fast momentum-based version (Beck & Teboulle, 2009).

Sparse ReLU autoencoders For shallow ReLU autoencoders (Bricken et al., 2023b), the formulation reduces to

$$\begin{aligned} \min_{\mathbf{D} \in \mathcal{D}} \quad & \frac{1}{2}\|\mathbf{x} - (\mathbf{D}\mathbf{z} + \mathbf{b}_{\text{pre}})\|_2^2 + \lambda\|\mathbf{z}\|_1 \\ \text{s.t.} \quad & \mathbf{z} = \text{ReLU}(\mathbf{W}^\top(\mathbf{x} - \mathbf{b}_{\text{pre}}) + \mathbf{b}_{\text{enc}}) \end{aligned} \quad (6)$$

This connection between bilevel optimization and neural networks, highlighted in (Tolooshams, 2023; Hindupur et al., 2025), has been explored extensively in the context of sparse autoencoders. Prior works have studied the gradient dynamics of variants of ReLU networks when the encoder is shallow (Nguyen et al., 2019; Arora et al., 2015; Rangamani et al., 2018) or deep, as in learned ISTA architectures (Tolooshams & Ba, 2022). Others have analyzed model recovery when the encoder is deep and iterative with hard-thresholding nonlinearity (JumpReLU (Rajamanoharan et al., 2024)) (Rambhatla et al., 2018).

Overall, optimizing or recovering sparse generative linear models has attracted sustained attention from two main deep learning communities over the past years; a) *Unrolling learning*: using optimization formulations to design and theoretically study neural architectures (Ablin et al., 2019; Mal  zieux et al., 2022; Tolooshams & Ba, 2022; Nguyen et al., 2019; Arora et al., 2015; Chen et al., 2018; Rangamani et al., 2018; Tolooshams et al., 2020; Rambhatla et al., 2018), and b) *Sparse interpretability* or mechanistic interpretability: leveraging sparse models to interpret and analyze the internal representations of complex larger networks (Elhage et al., 2022; Huben et al., 2023; Bricken et al., 2023b; Rajamanoharan et al., 2024; Park et al., 2024; Templeton et al., 2024; Lieberum et al., 2024; Gao et al., 2025; Fel et al., 2025; Marks et al., 2025; Karvonen et al., 2025). We briefly expand on both works.

Unrolled learning The early connections between sparse coding and deep learning trace back to sparse energy-based deep models (Ranzato et al., 2007; 2008) and the pioneering work of LISTA (Gregor & LeCun, 2010) in constructing sparsifying recurrent neural networks. This line of work, known as unfolding (Hershey et al., 2014) or unrolling (Monga et al., 2021), designs neural network layers based on iterations of an algorithm that solves an optimization problem. This connection has enabled researchers to use optimization models as a proxy to theoretically study accelerated convergence (Chen et al., 2018; Ablin et al., 2019), gradient dynamics (Arora et al., 2015; Rangamani et al., 2018; Nguyen et al., 2019; Tolooshams et al., 2020), and model recovery in both shallow (Arora et al., 2015) and deep neural networks (Rambhatla et al., 2018; Tolooshams & Ba, 2022). Furthermore, several works have explored the theoretical connections between convolutional neural networks and convolutional sparse coding (Papayan et al., 2017a,b), or more generally, between deeply sparse signal representations and deep neural networks (Ba, 2020). An example of a deep unrolled JumpReLU neural network for sparse model recovery can be formulated as the following bilevel optimization problem.

$$\min_{\mathbf{D} \in \mathcal{D}} \quad \|\mathbf{x} - \mathbf{D}\mathbf{z}_T\|_2^2 \quad \text{s.t.} \quad \mathbf{z}_t = \text{JumpReLU}_\lambda(\mathbf{z}_{t-1} - \alpha\mathbf{D}^\top(\mathbf{D}\mathbf{z}_{t-1} - \mathbf{x})) \quad (7)$$

for $t = 1, \dots, T$, where $\mathbf{z}_0 = \mathbf{0}$, α is the step size, and $\text{JumpReLU}_\lambda(\mathbf{z}) = \mathbf{z} \cdot \mathbb{1}_{\mathbf{z} > \lambda}$, where $\mathbb{1}$ is the indicator function, and λ controls the sparsity level of the representation. The inner mapping is now a deep/iterative encoder, which for simplicity

we denote by $z_T = f_\theta(\mathbf{x})$. The outer objective enforces the structure of the decoder and the loss function. The bilevel optimization in Equation (7) can be mapped to the following neural network autoencoder architecture, which uses a recurrent and residual encoder. The synthetic experiments in this paper use this encoder in its architecture for sparse model recovery.

$$\begin{aligned} \text{(encoder)} \quad z_t &= \text{JumpReLU}_\lambda(z_{t-1} - \alpha \mathbf{D}^\top (\mathbf{D} z_{t-1} - \mathbf{x})), \quad \text{for } t = 1, \dots, T \\ \text{(decoder)} \quad \hat{\mathbf{x}} &= \mathbf{D} z_T. \end{aligned} \quad (8)$$

For experiments recovering the sparse convolutional generative model, we use the architecture that takes convolution blocks, as shown below.

$$\begin{aligned} \text{(encoder)} \quad z_{c,t} &= \text{JumpReLU}_\theta(z_{c,t-1} - \alpha \mathbf{D}_c \star (\sum_{c=1}^C \mathbf{D}_c * z_{c,t-1} - \mathbf{x})), \quad \text{for } t = 1, \dots, T \\ \text{(decoder)} \quad \hat{\mathbf{x}} &= \mathbf{D} * z_T \end{aligned} \quad (9)$$

for $t = 1, \dots, T$ and $c = 1, \dots, C$, where $z_0 = \mathbf{0}$, α is the step size, $*$ is convolution operator, and \star is a correlation operator.

Convolutional Setting Sparse generative models can be extended to *sparse convolutional generative models* (Definition A.1), where the concepts are locally and sparsely appearing in the data.

Definition A.1 (Sparse Convolutional Generative Models). A data example $\mathbf{x} \in \mathbb{R}^m$ is said to follow a sparse convolutional generative model if there exists a sparse latent representation $\mathbf{z} = \{z_c \in \mathbb{R}^p\}_{c=1}^C$ (with $\text{supp}(z_c) \leq k \ll p$) and a set of C localized dictionary $\{\mathbf{D}_c^* \in \mathbb{R}^h\}_{c=1}^C$ (with $h \ll m$) such that $\mathbf{x} = \sum_{c=1}^C \mathbf{D}_c^* * z_c$ in the noiseless setting, where $*$ denotes the convolution operator.

Neural operators Neural operators consist of the following three modules:

- **Lifting:** This is a fully local operator which we model by a matrix $\mathbf{L} : \mathbb{R}^m \rightarrow \mathbb{R}^{d_{v_0}}$. It maps the input $\{\mathbf{x} : D_x \rightarrow \mathbb{R}^m\}$ into a latent representation $\{v_0 : D_0 \rightarrow \mathbb{R}^{d_{v_0}}\}$, where $h > m$.
- **Kernel Integration:** For $t = 0, \dots, T-1$, this is a non-local integral kernel operator that maps representation at one layer $\{v_t : D_t \rightarrow \mathbb{R}^{d_{v_t}}\}$ to the next $\{v_{t+1} : D_{t+1} \rightarrow \mathbb{R}^{d_{v_{t+1}}}\}$ (see Definition A.2).
- **Projection:** This is a fully local operator, similar to the lifting operator. It maps the filtered lifted data to the output function, i.e., $\mathbf{P} : \mathbb{R}^{d_{v_T}} \rightarrow \mathbb{R}^m$, where $d_{v_T} > m$.

where the kernel integral operator is used to map \mathbf{x} to an estimate of the representation \mathbf{z} , the input/output domains would be D_x and D_z , respectively. Moreover, when the kernel integral operator is used to refine the latent representation \mathbf{z} from one layer to another, the input/output domain of the operator would be both D_z .

Definition A.2 (Kernel integral operator \mathcal{K} (restated from (Kovachki et al., 2023))). Define the kernel integral operator by

$$(\mathcal{K}_t(v_t))(x) := \int_{D_t} \kappa^{(t)}(x, y) v_t(y) dv_t(y), \quad \forall x \in D_{t+1} \quad (10)$$

where $\kappa^{(t)} : C(D_{t+1} \times D_t; \mathbb{R}^{d_{v_{t+1}} \times d_{v_t}})$ are the parameters of the kernels, modeled by a neural network, and v_t is a Borel measure on D_t , where C denotes the space of continuous functions.

Definition A.3 (Fourier integral operator \mathcal{K} (restated from (Kovachki et al., 2023))). Define the Fourier integral operator by

$$(\mathcal{K}(\phi)v_t)(\mathbf{x}) = \mathcal{F}^{-1}(R_\phi \cdot (\mathcal{F}v_t))(\mathbf{x}), \quad \forall \mathbf{x} \in D \quad (11)$$

where $R_\phi := \mathcal{F}(\kappa)$ is the Fourier transform of a periodic function $\kappa : D \rightarrow \mathbb{C}^{d_w \times d_v}$ parameterized by ϕ .

Fourier neural operator (FNO) (Li et al., 2021) models the kernel integral operator with a convolution operator parameterized in Fourier space (Definition A.3, see also Definition A.4 for Fourier transform). The convolution operator parameterizes the kernel $\kappa(x, y) = \kappa(x - y)$ as a complex function $\kappa : D \rightarrow \mathbb{C}^{d_w \times d_v}$. FNO is used with truncated frequency modes in practice; this has been shown to improve performance and lower sensitivity to change (decreasing) the discretization sampling (Li et al., 2021; Kovachki et al., 2023).

Definition A.4 (Fourier transform). Let \mathcal{F} the Fourier transform of the function $\mathbf{v} : D \rightarrow \mathbb{R}^{d_v}$, whose inverse is denoted by \mathcal{F}^{-1} on the function $\mathbf{w} : D \rightarrow \mathbb{C}^{d_w}$. We have

$$\begin{aligned} (\mathcal{F}\mathbf{v})_j(k) &= \int_D \mathbf{v}_j(x) e^{-2i\pi\langle x, k \rangle} dx, & j = 1, \dots, d_v \\ (\mathcal{F}^{-1}\mathbf{w})_j(x) &= \int_D \mathbf{w}_j(k) e^{2i\pi\langle x, k \rangle} dk, & j = 1, \dots, d_w \end{aligned} \quad (12)$$

where $i = \sqrt{-1}$ is the imaginary unit.

B. Appendix - Additional Experimental Results

B.1. Experimental Setup

Sparse Generative Model The results shown in Figure 10 are from a synthetic dataset that follows a sparse generative model (Definition 2.1). The atoms of the ground-truth dictionary $\mathbf{D}^* \in \mathbb{R}^{1000 \times 1500}$ are drawn from a standard normal distribution and then ℓ_2 -normalized. The dataset consists of 50,000 samples $\mathbf{x} \in \mathbb{R}^{1000}$. Each latent code $\mathbf{z} \in \mathbb{R}^{1500}$ has a total sparsity of 20. The amplitudes of the non-zero elements are drawn from a sub-Gaussian distribution with a mean of 15 and a standard deviation of 1.0.

SAE For both SAE (SAE-MLP) and L-SAE (L-SAE-MLP) models, the encoder implements $f_\theta(\mathbf{x})$ following Definition 2.2 using a deep unrolled JumpReLU network (eq. 7.8) with $T = 50$ layers, as described in the sparse model recovery framework (Definition 2.2). The non-linearity is Hard-Thresholding with a threshold of $\lambda = 0.5$, and the algorithm’s internal step-size is $\alpha = 0.2$. The decoder reconstructs data as $\hat{\mathbf{x}} = \mathbf{D}\mathbf{z}$ following Definition 2.3. The dictionary weights for both SAE and L-SAE are initialized with a noisy ($\sigma = 0.02$) version of the ground-truth dictionary. For the L-SAE, the 1000-dimensional input is lifted to a 1200-dimensional space. Both models are trained to minimize the Mean Squared Error (MSE) reconstruction loss using the SGD optimizer with a learning rate of $\eta = 10^{-3}$.

Sparse Convolutional Generative Model The results for convolutional dictionary are from a synthetic dataset that follows a sparse convolutional generative model (Definition A.1). The ground-truth dictionary \mathbf{D}^* consists of $p = 5$ kernels with spatial support $h = 99$. Each kernel is a multi-channel signal with 64 input channels. The values for each kernel are drawn from a standard normal distribution and then normalized. The dataset consists of 50,000 samples $\mathbf{x} \in \mathbb{R}^{64 \times 1000}$. Each sample is generated by convolving a single (i.e., sparsity of 1) randomly chosen kernel from the dictionary with a sparse feature map, whose non-zero amplitudes are drawn from a sub-Gaussian distribution.

SAE-CNN For both SAE-CNN and L-SAE-CNN models, the encoder implements the convolutional version of the a deep unrolled network (Equation (9)) with $T = 50$ layers, as described in the sparse model recovery framework (Definition 2.2). The non-linearity is Hard-Thresholding with a threshold of $\lambda = 10$, and the algorithm’s internal step-size is $\alpha = 0.01$. The dictionary kernels for both SAE-CNN and L-SAE-CNN are initialized with a noisy ($\sigma = 0.05$) version of the ground-truth kernels. For L-SAE-CNN, the 64-channel input is lifted to a 128-dimensional space. Both models are trained to minimize the Mean Squared Error (MSE) reconstruction loss using the SGD optimizer with a learning rate of $\eta = 0.04$.

SAE-FNO For both SAE-FNO and L-SAE-FNO models, the encoder implements a deep unrolled network with $T = 50$ layers, as described in the sparse functional model recovery framework (Definition 3.2). The non-linearity is Hard-Thresholding with a threshold of $\lambda = 10$, and the algorithm’s internal step-size is $\alpha = 0.01$. The dictionary kernels are initialized with a noisy ($\sigma = 0.05$) version of the ground-truth. For L-SAE-FNO, the 64-channel input is lifted to a 128-dimensional space. Both SAE-FNO and L-SAE-FNO are trained to minimize the Mean Squared Error (MSE) reconstruction loss using the SGD optimizer with a learning rate of $\eta_L = 20.04$.

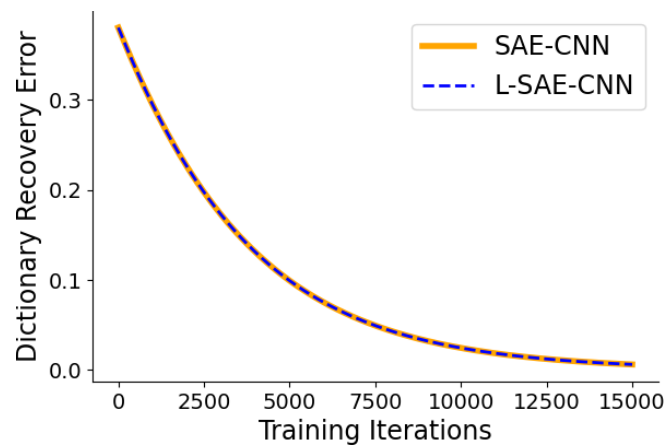


Figure 9. **Lifting**. Learning when $L^T L = I$.

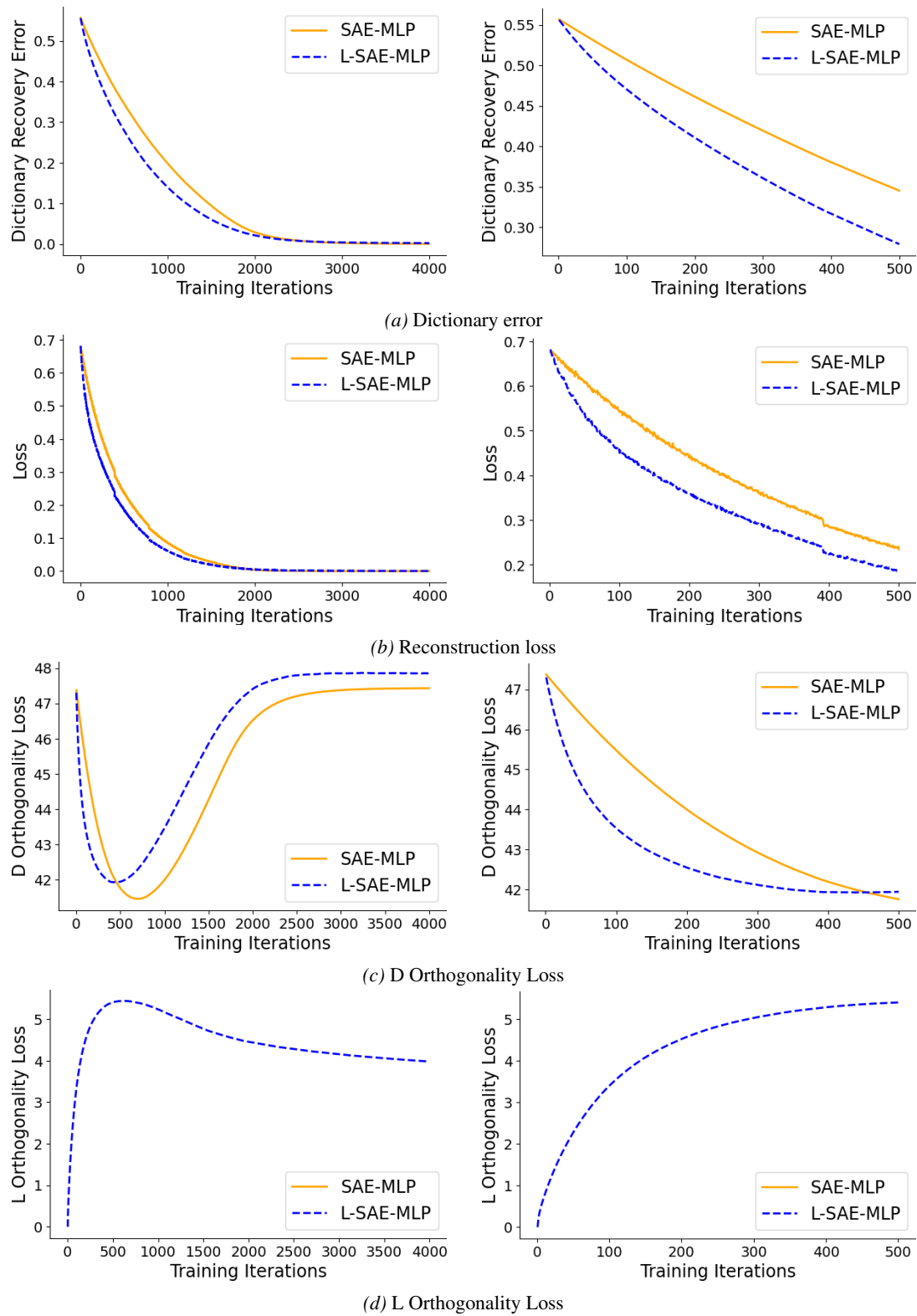


Figure 10. SAEs vs. L-SAEs. Learning the lifting operator L accelerates model recovery.

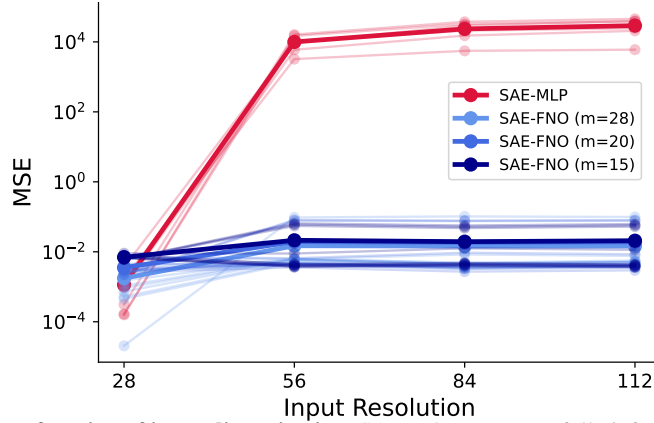


Figure 11. SAE-FNO vs. SAE as a function of input discretization. SAE-NO can successfully infer the underlying representations that allow it to reconstruct data at varying resolution beyond the original trained resolution of 28. The figure shows MSE on the reconstruction.

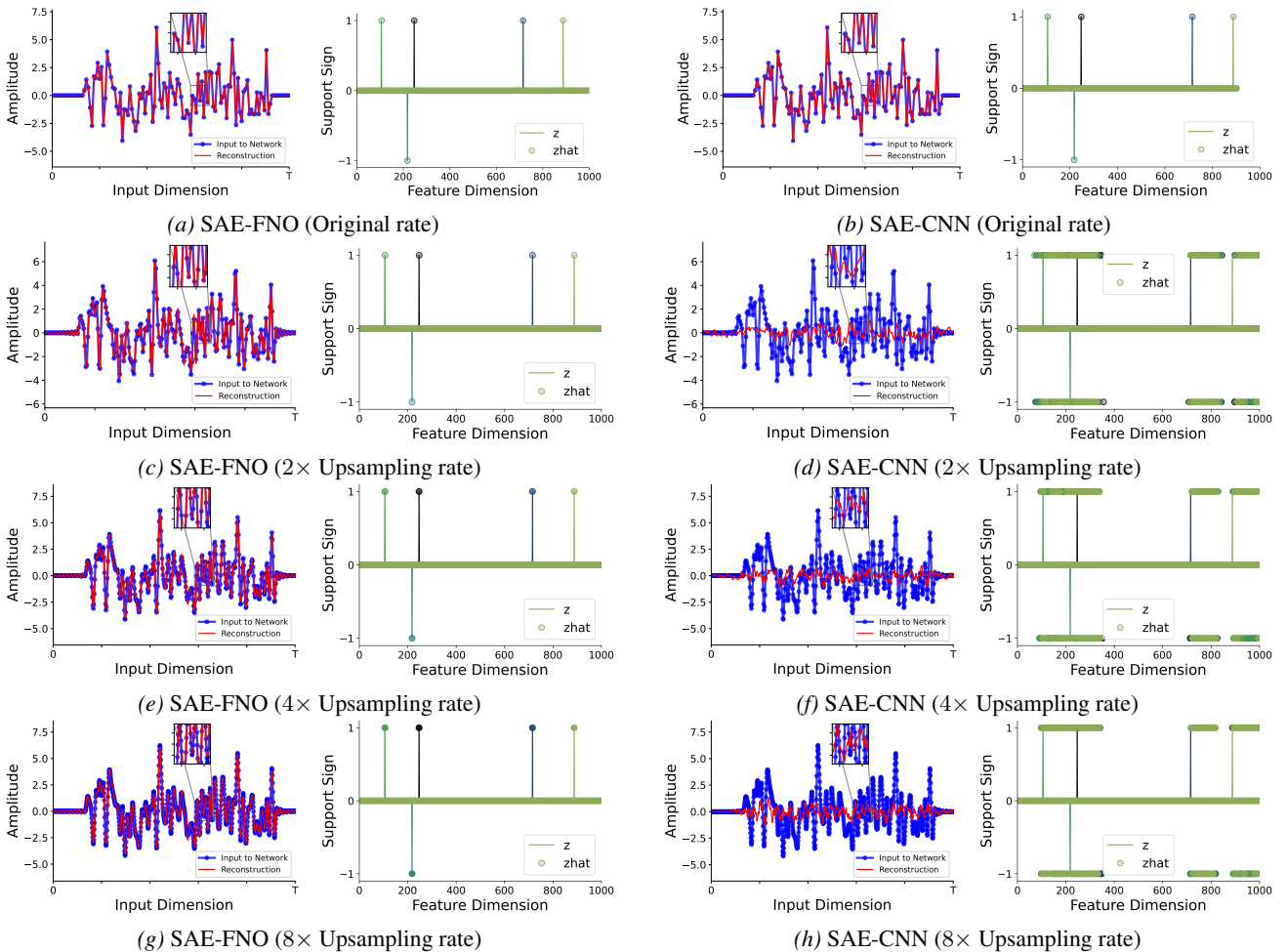


Figure 12. SAE-FNO Upsampling Robustness Across Resolutions. We evaluate the ability of SAE-FNO (left column) and SAE-CNN (right column) to infer sparse representations and reconstruct data across varying discretization levels. Each row represents a different upsampling rate (1 \times to 8 \times applied to the input signal). For each panel, the left plot shows the spatial-domain signal reconstruction (red) against the input to the network (blue), and the right plot shows the inference of 1-sparse code supports across 5 kernels. (a-b) Original resolution (1 \times): Baseline performance at training resolution. Both models accurately reconstruct the signal and recover the correct support. (c-h) Higher upsampling rates (2 \times , 4 \times , 8 \times): As spatial resolution increases, SAE-FNO maintains accurate reconstruction and code support inference. In contrast, SAE-CNN fails to generalize; its support inference collapses, leading to poor reconstruction. The SAE-FNO’s function space parameterizations enables this generalization across discretizations.

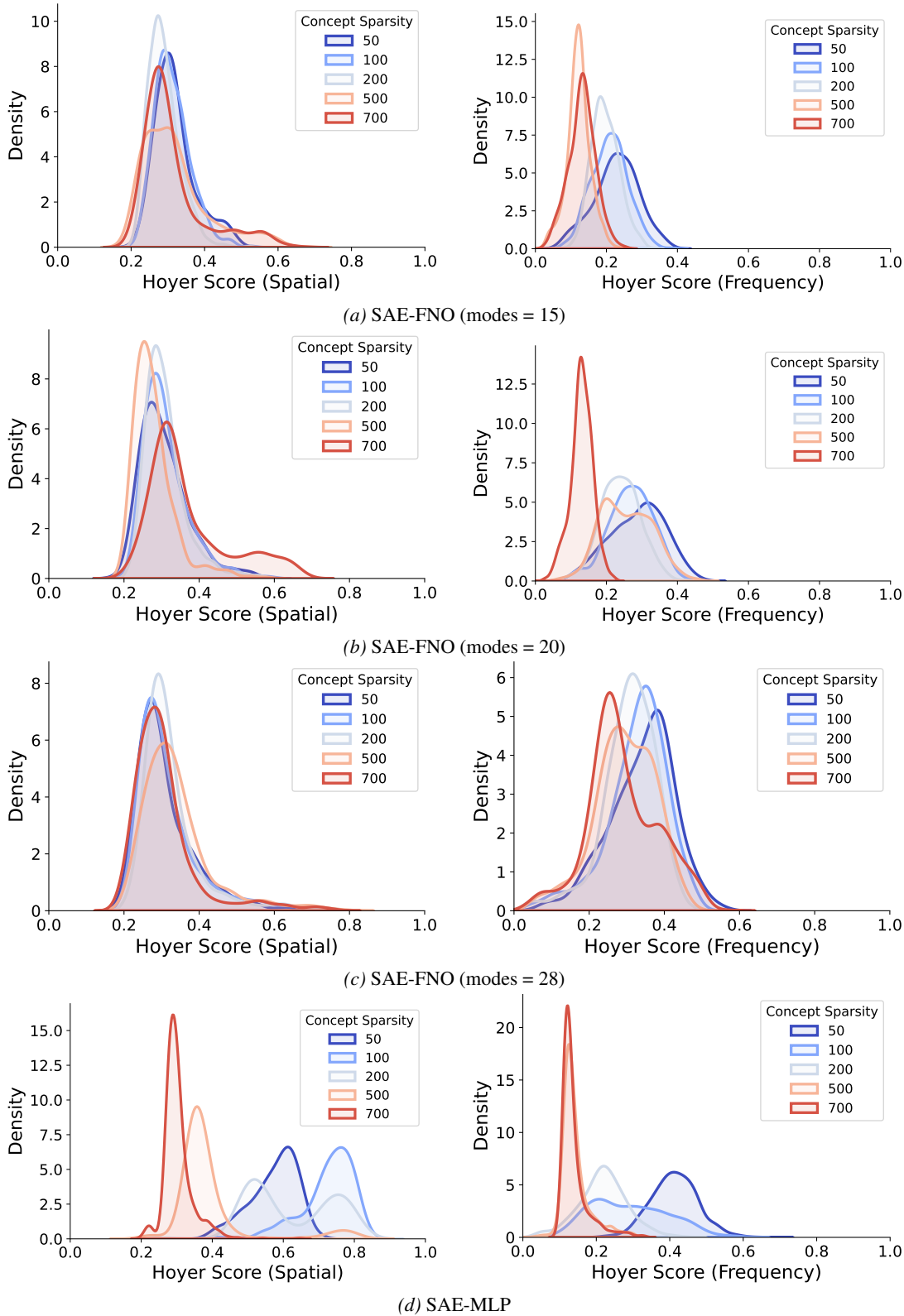


Figure 13. Stability of concept characteristics across concept sparsity levels (MNIST). We evaluate the stability of learned concepts of SAE-MLP and SAE-FNO (with spatial sparsity 0.007) by computing the distribution of their Hoyer scores in both the spatial and frequency domains, across varying concept sparsity constraints ($k \in [50, 700]$). The y-axis represents the probability density normalized such that the area under the curve equals 1. (a-c) SAE-FNO stability: The distribution of both spatial and frequency Hoyer score remains consistent as k varies, regardless of the number of Fourier modes used. (d) SAE-MLP instability: the distributions for SAE-MLP shift drastically with changes in k , indicating that the characteristics of learned atoms are highly sensitive to the concept sparsity constraint.

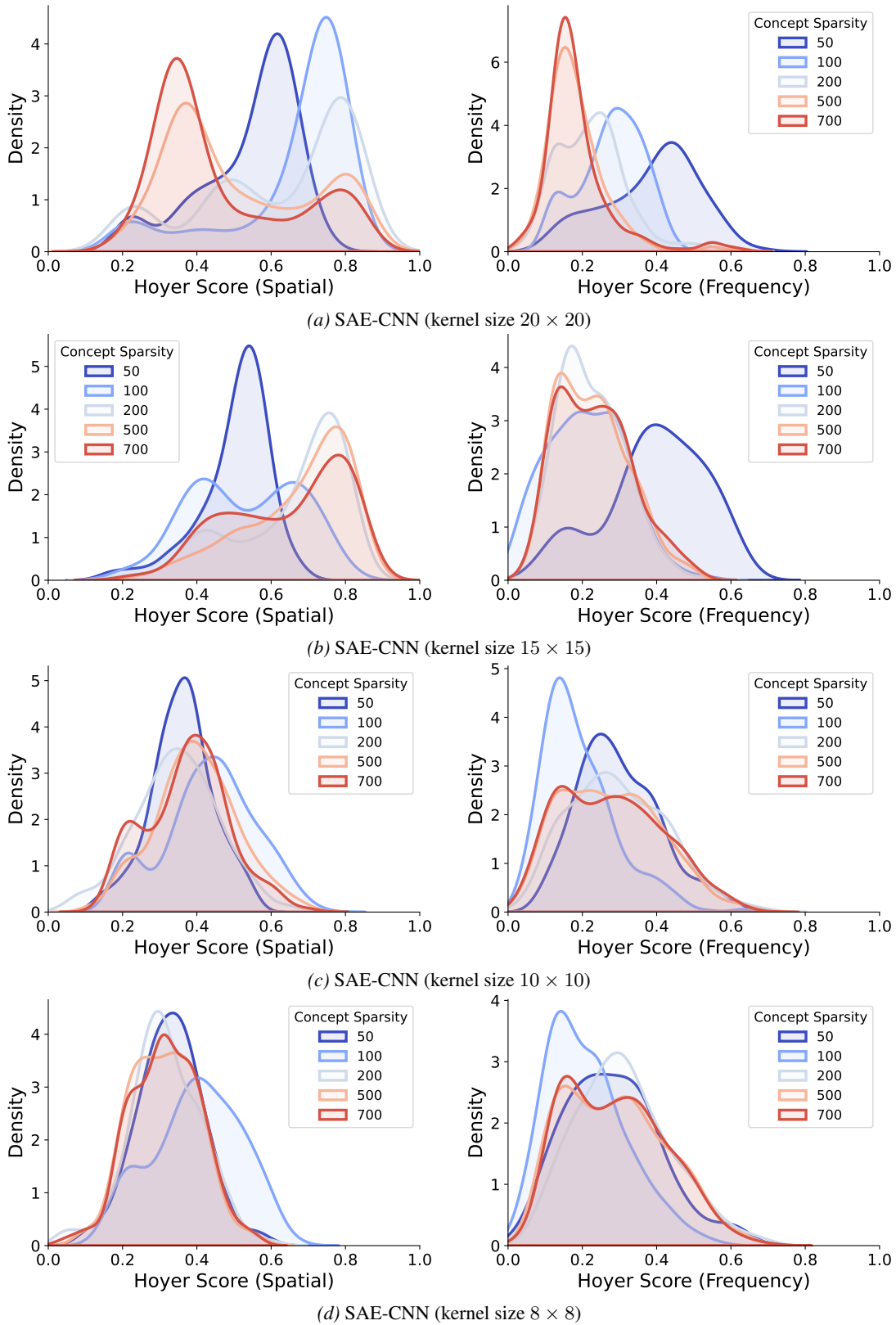


Figure 14. Effect of kernel size on SAE-CNN concept stability (MNIST). We examine Hoyer score densities for SAE-CNN architectures with decreasing kernel sizes. As the kernel size decreases from 20×20 to 8×8 , the distributions of atom sparsity become increasingly stable across concept sparsity values. This is expected as restricting the receptive field imposes a stronger inductive bias for locality. Smaller kernels force the network to learn more consistent and localized features.

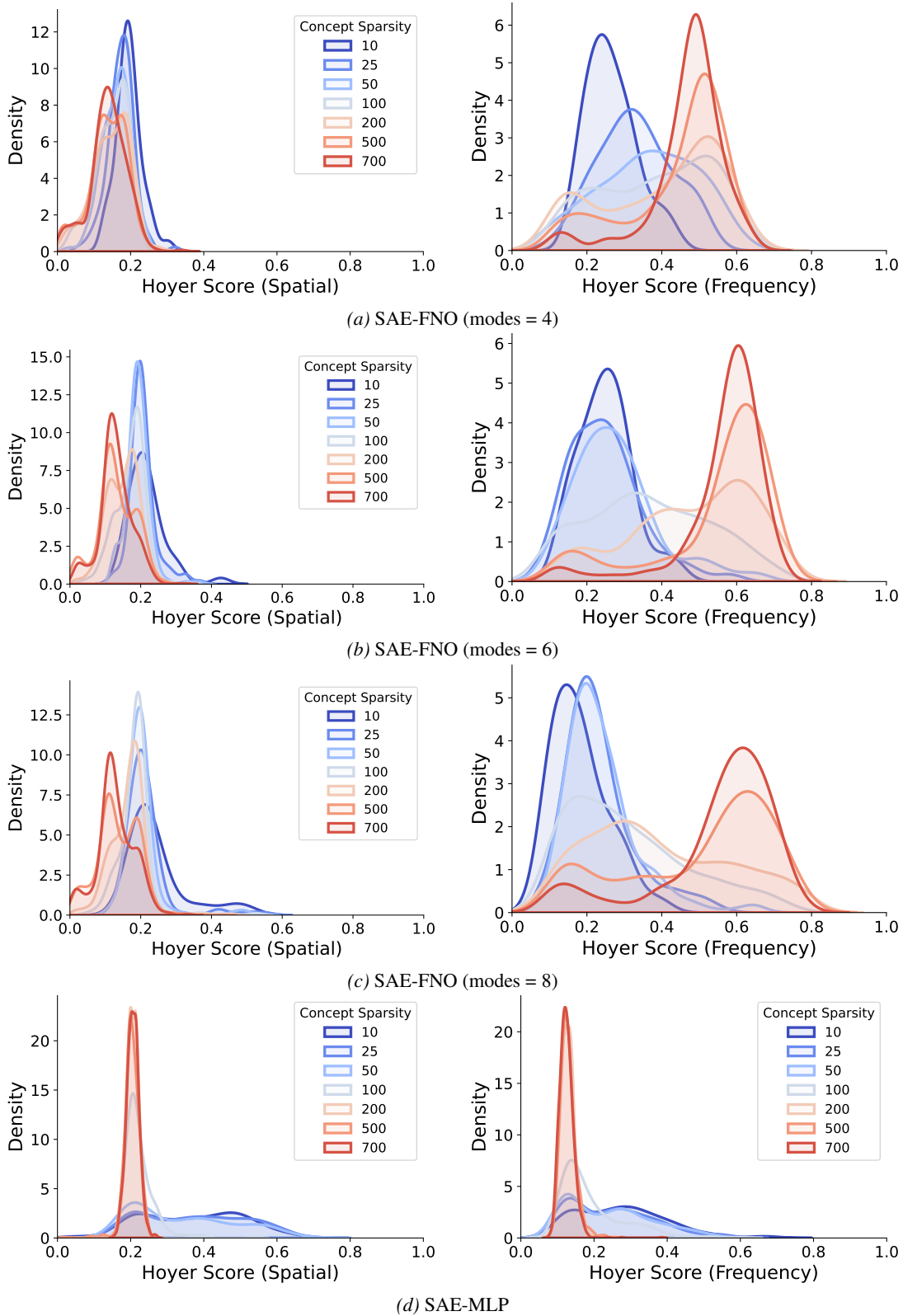


Figure 15. **Stability of concept characteristics across concept sparsity levels (CIFAR).** CIFAR Hoyer scores for SAE-MLP and SAE-FNO (ss = 0.005, 3-sparse)

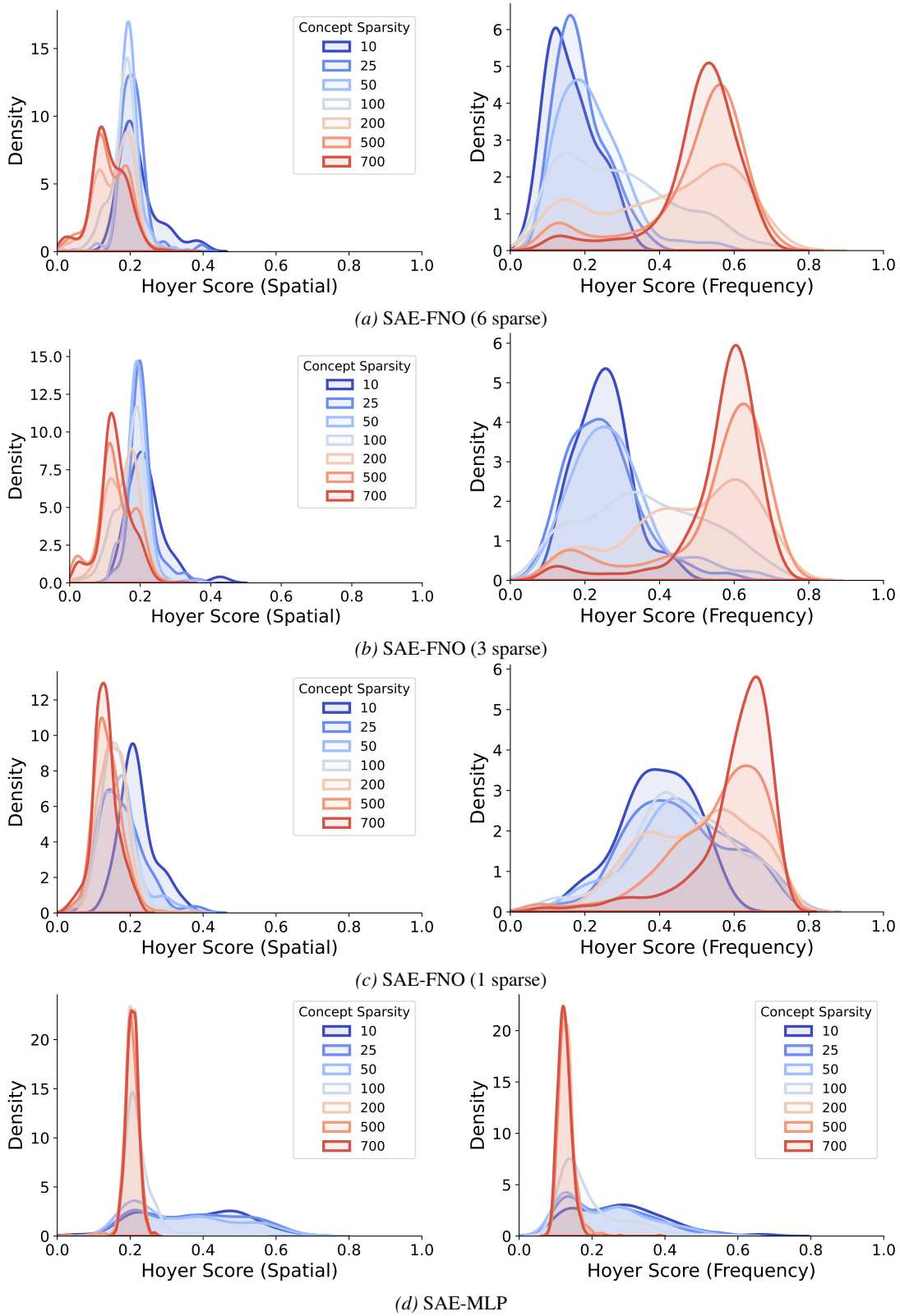


Figure 16. Concept characterization in CIFAR. Hoyer scores for SAE-MLP and SAE-FNO (modes = 6).

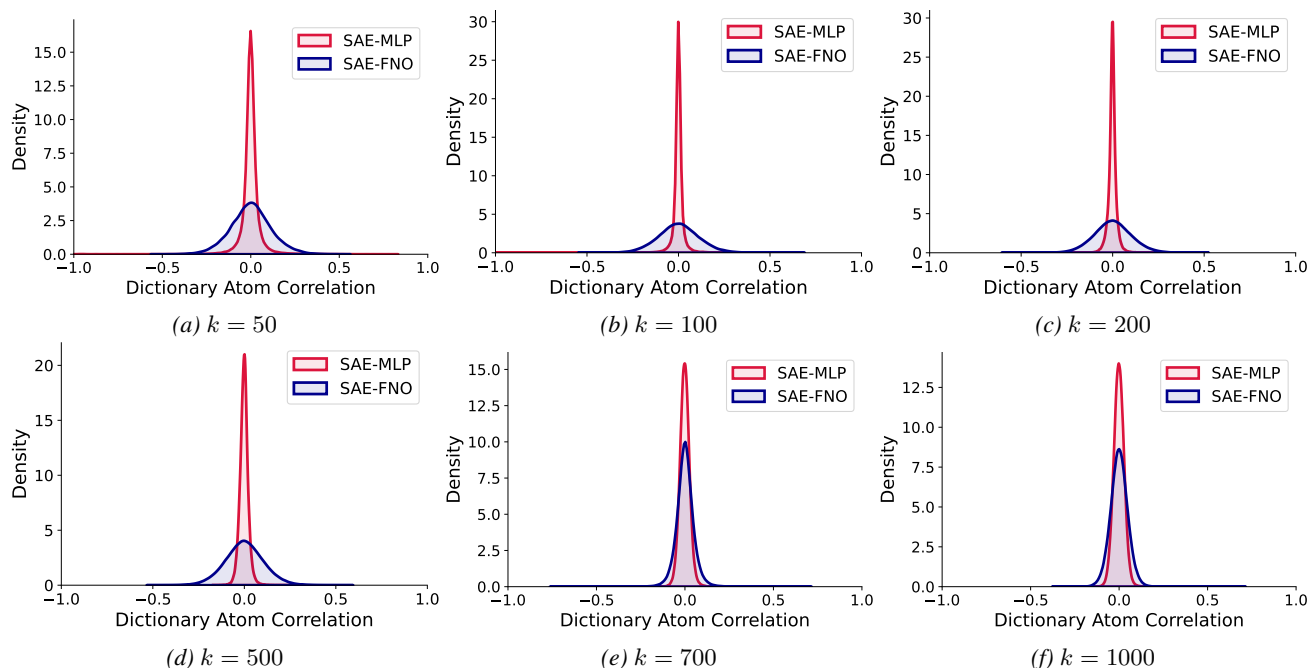


Figure 17. SAE-FNO overcomes orthogonality bias and recovers correlated concepts in MNIST. We compare the distribution of pairwise cosine similarities (correlations) between learned dictionary atoms for SAE-FNO (blue) and SAE-MLP (red) across varying concept sparsity levels (k). SAE-FNOs display a broader distribution with heavier tails, indicating a better ability to recover non-orthogonal, correlated concepts.

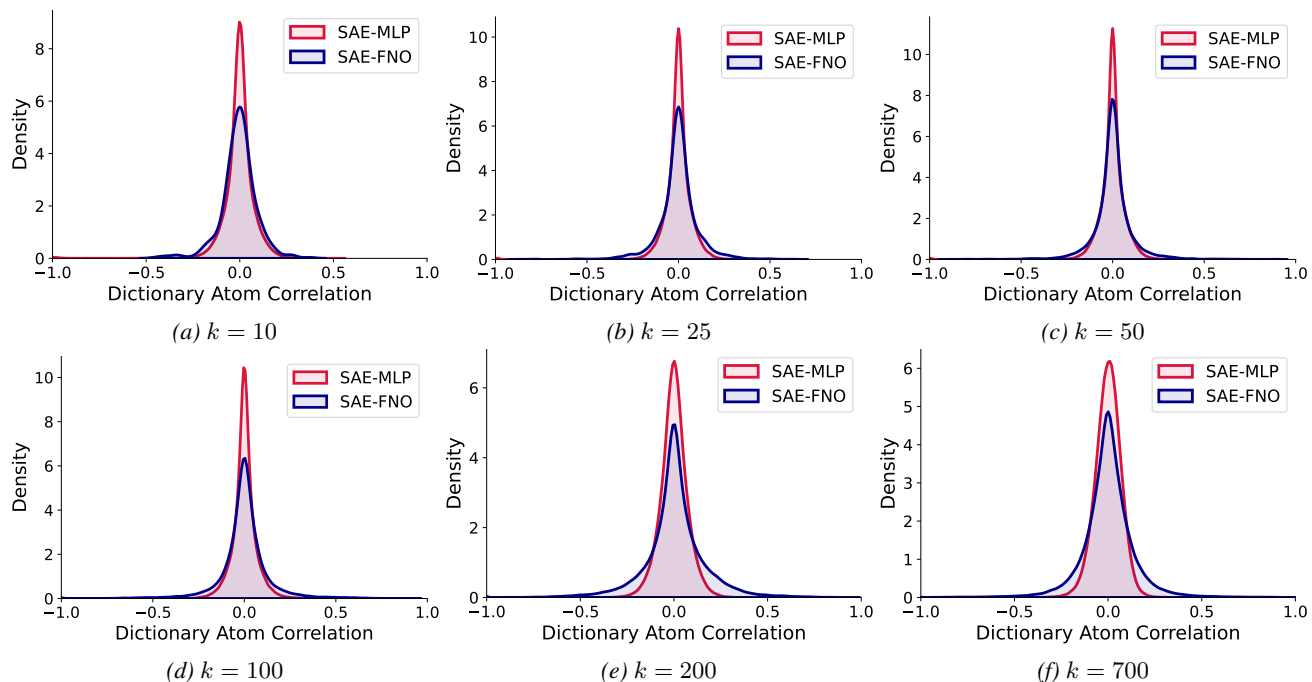


Figure 18. SAE-FNO overcomes orthogonality bias and recovers correlated concepts in CIFAR. Similar to the MNIST results, we compare the distribution of pairwise cosine similarities between learned dictionary atoms for SAE-FNO (blue) and SAE-MLP (red) across varying concept sparsity levels (k). The SAE-FNO models use 6 Fourier modes and a spatial sparsity of 0.02. SAE-FNO consistently displays a broader correlation distribution with heavier tails compared to SAE-MLP.

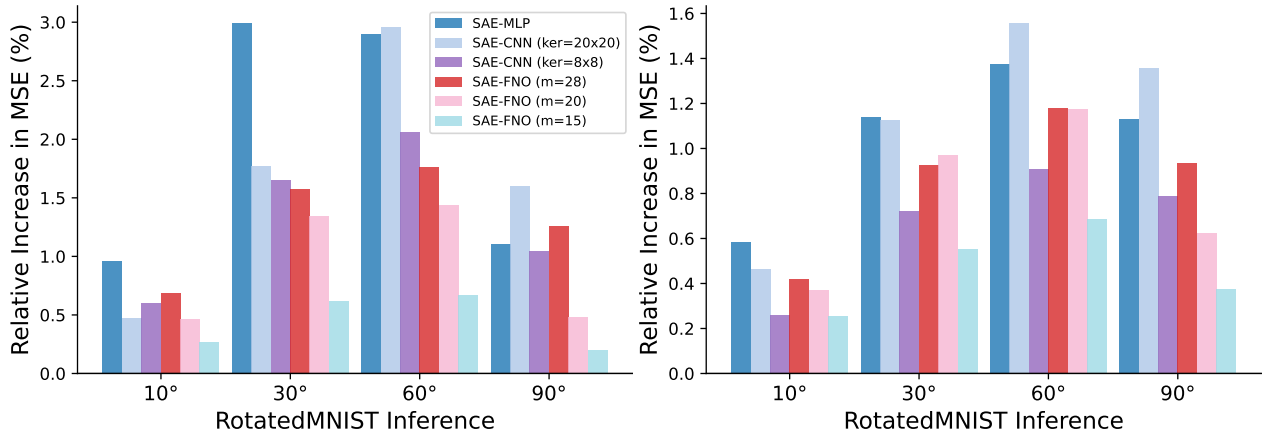


Figure 19. FNO generalizes well out-of-distribution compared to SAE-MLP and SAE-CNN. Left: $p = 1000$. Right: $p = 256$.

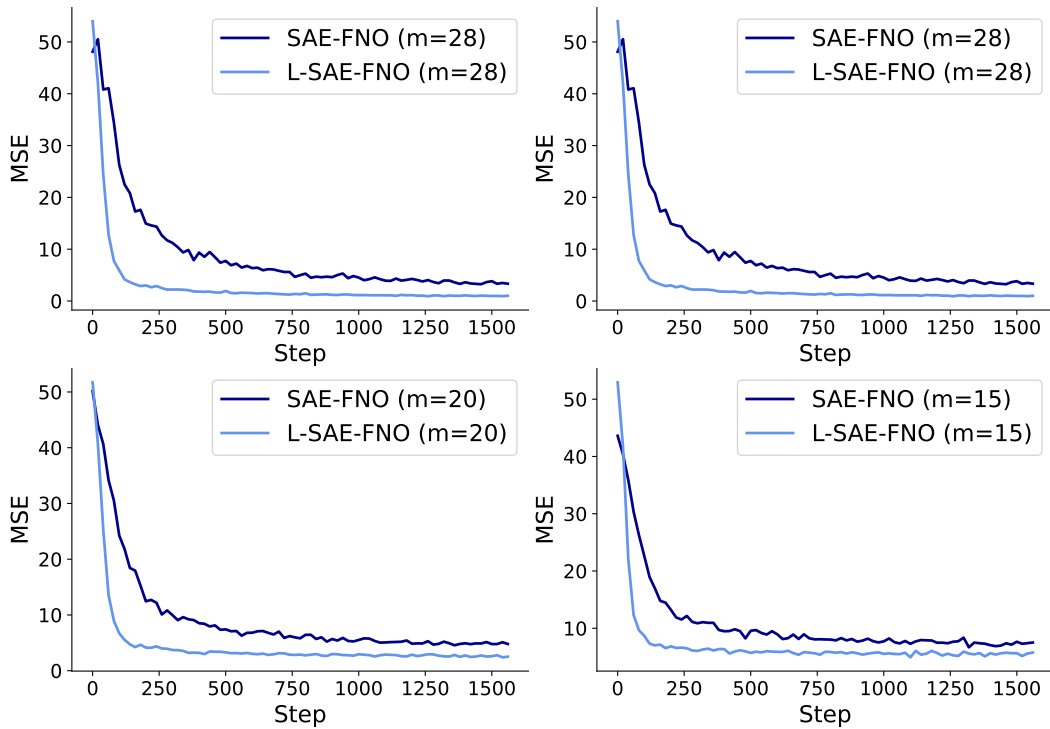


Figure 20. Lifting accelerates learning. MNIST.

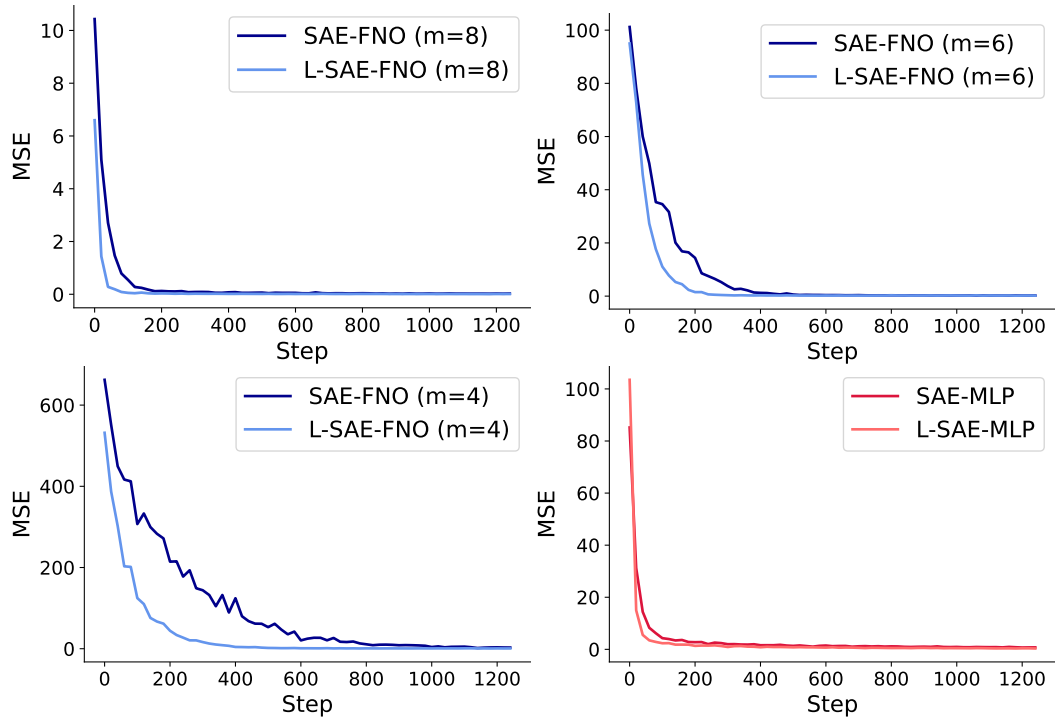


Figure 21. Lifting accelerates learning. CIFAR.

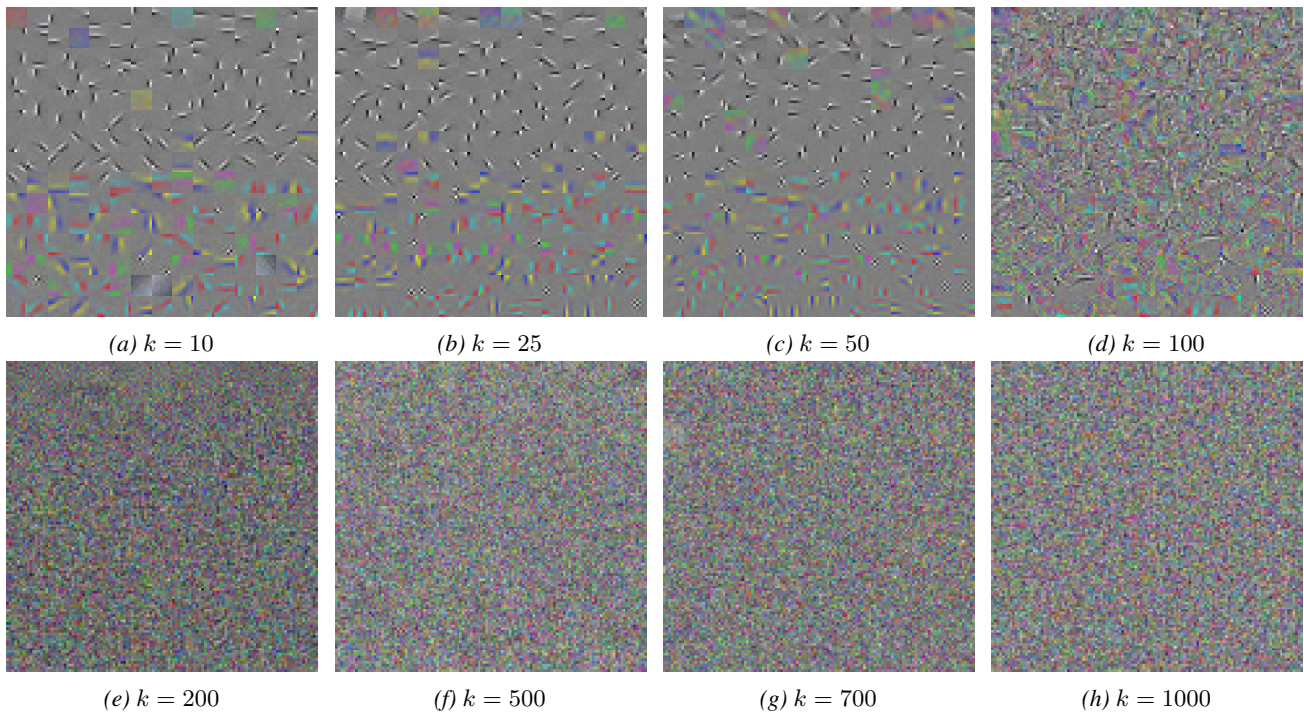


Figure 22. Additional visualizations. SAE-MLP learned concepts on CIFAR.

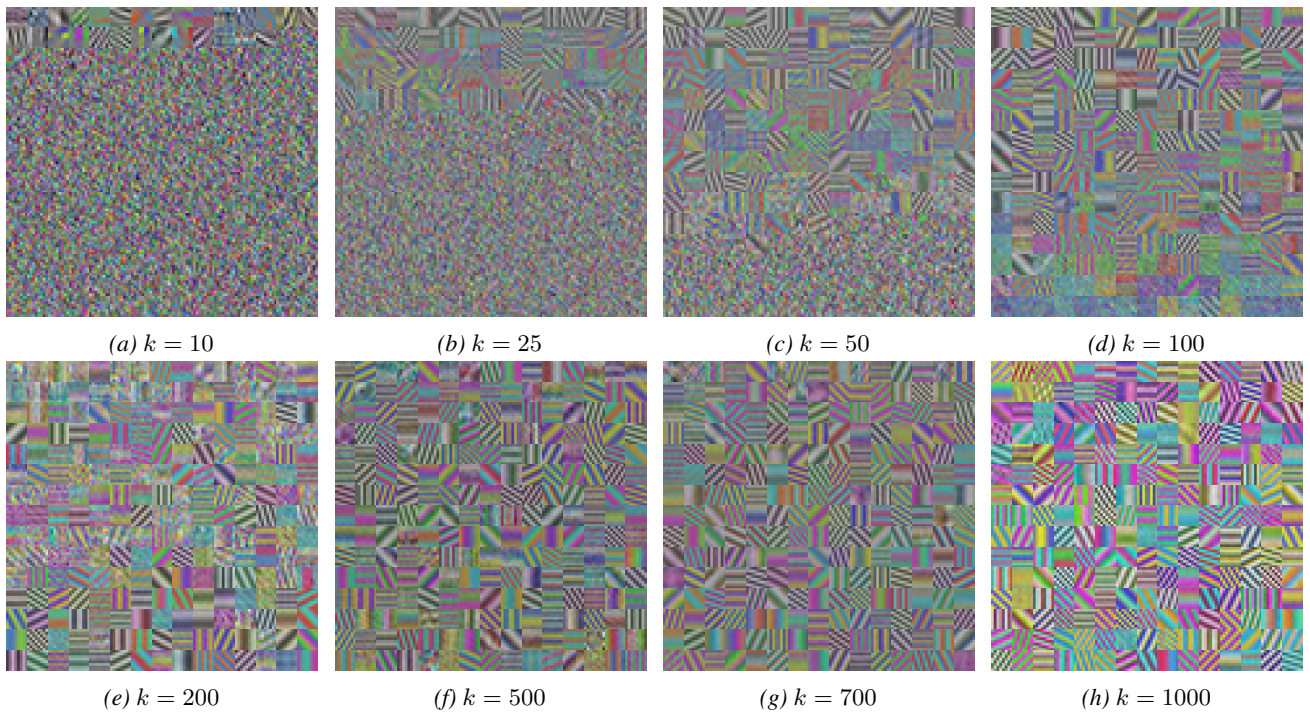


Figure 23. **Additional visualizations** SAE-FNO (modes = 6, spatially 1-sparse) learned concepts on CIFAR.

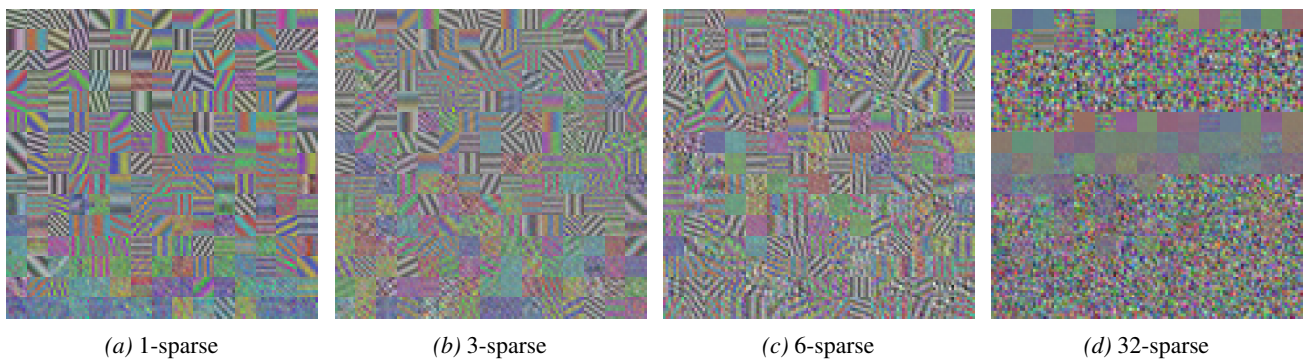


Figure 24. **Additional visualizations.** SAE-FNO (modes = 6) learned concepts on CIFAR as spatial sparsity changes.

C. Appendix - Theoretical Analysis

This section provides the mathematical derivations for the training dynamics of the architectures discussed in the main text. We derive the gradient descent update rules for a single data sample, which are used to learn the dictionary parameters. These derivations consider the *analytic gradient*, i.e., the dictionary gradient is computed given the codes (Malézieux et al., 2022; Tolooshams & Ba, 2022).

Proposition C.1 (Architectural Inference Equivalence of Lifting in SAE). *The architectural inference of a SAE is equivalent to a lifted-SAE if the projection is tied to the lifting operator ($\mathbf{P} = \mathbf{L}^\top$), and the lifting operator is orthogonal ($\mathbf{L}^\top \mathbf{L} = \mathbf{I}$), i.e., under the same learned model $\mathbf{D} = \mathbf{P}\mathbf{D}_L$, the representation dynamics and output of the networks are equivalent.*

Proof. We provide the proof for the sparse generative model case when the encoder implements a proximal gradient descent type of operation in an unrolled learning setting (e.g., 8). For the SAE, the representation refinement at every encoder layer follows:

$$\mathbf{z}_{t+1} = \mathcal{R}(\mathbf{z}_t - \alpha \mathbf{D}^\top (\mathbf{D}\mathbf{z}_t - \mathbf{x})) \quad (13)$$

By construction, we incorporate the underlying model from the lifted-SAE to the standard SAE: $\mathbf{D} = \mathbf{P}\mathbf{D}_L$, and re-write the encoder as:

$$\mathbf{z}_{t+1} = \mathcal{R}(\mathbf{z}_t - \alpha (\mathbf{P}\mathbf{D}_L)^\top (\mathbf{P}\mathbf{D}_L\mathbf{z}_t - \mathbf{x})) = \mathcal{R}(\mathbf{z}_t - \alpha \mathbf{D}_L^\top \mathbf{P}^\top (\mathbf{P}\mathbf{D}_L\mathbf{z}_t - \mathbf{x})) \quad (14)$$

Using the assumption on the lifting-projection,

$$\mathbf{z}_{t+1} = \mathcal{R}(\mathbf{z}_t - \alpha (\mathbf{D}_L)^\top (\mathbf{D}_L\mathbf{z}_t - \mathbf{L}\mathbf{x})) \quad (15)$$

This final expression is the iterative encoder update for \mathbf{z} in the lifted space, where the dictionary is \mathbf{D}_L and the input is lifted by \mathbf{L} . This completes the proof of architectural inference equivalence on the standard and lifted architectures. ■

Proposition C.2 (Training Dynamics of Lifting). *The training dynamics of the lifted-SAE (L-SAE) $\mathbf{D}_L^{(k+1)} = \mathbf{D}_L^{(k)} + \eta \mathbf{P}^\top (\mathbf{x} - \mathbf{P}\mathbf{D}_L^{(k)}\mathbf{z})\mathbf{z}^\top$, with lifting \mathbf{L} and projection \mathbf{P} , has the effective update in the original space, expressed as: $\mathbf{D}^{(k+1)} = \mathbf{D}^{(k)} + \eta \mathbf{L}(\mathbf{L}^\top \mathbf{L})(\mathbf{x} - \mathbf{D}^{(k)}\mathbf{z})\mathbf{z}^\top$, where $\mathbf{L}^\top \mathbf{L}$ acts as a preconditioner, potentially accelerating learning by inducing a more isotropic update. If they satisfy the equivalent architectural inference (Proposition C.1), then the dynamics are equivalent to those of an SAE: $\mathbf{D}^{(k+1)} = \mathbf{D}^{(k)} + \eta(\mathbf{x} - \mathbf{D}^{(k)}\mathbf{z})\mathbf{z}^\top$.*

Proof. For the SAE, we learn a dictionary \mathbf{D} by minimizing the reconstruction loss for the data sample \mathbf{x} . The loss function is:

$$\mathcal{L}(\mathbf{D}) = \frac{1}{2} \|\mathbf{x} - \mathbf{D}\mathbf{z}\|_2^2 \quad (16)$$

The gradient of the loss for \mathbf{D} is:

$$\frac{\partial \mathcal{L}}{\partial \mathbf{D}} = -(\mathbf{x} - \mathbf{D}\mathbf{z})\mathbf{z}^\top \quad (17)$$

The analytic gradient update, given \mathbf{z} , for \mathbf{D} at iteration k with a learning rate η is therefore:

$$\mathbf{D}^{(k+1)} = \mathbf{D}^{(k)} - \eta \frac{\partial \mathcal{L}}{\partial \mathbf{D}^{(k)}} = \mathbf{D}^{(k)} + \eta(\mathbf{x} - \mathbf{D}^{(k)}\mathbf{z})\mathbf{z}^\top \quad (18)$$

For lifted-SAE, we learn a dictionary $\mathbf{D}_L \in \mathbb{R}^{h \times p}$ in a higher-dimensional lifted space. The input \mathbf{x} is lifted by $\mathbf{L} \in \mathbb{R}^{h \times m}$ and the reconstruction is projected back by $\mathbf{P} \in \mathbb{R}^{m \times h}$.

The loss function is defined in the original data space:

$$\mathcal{L}(\mathbf{D}) = \frac{1}{2} \|\mathbf{x} - \mathbf{P}\mathbf{D}_L\mathbf{z}\|_2^2 \quad (19)$$

The analytic gradient given \mathbf{z} of the loss with respect to \mathbf{D}_L is:

$$\frac{\partial \mathcal{L}}{\partial \mathbf{D}} = -\mathbf{P}^\top (\mathbf{x} - \mathbf{P}\mathbf{D}_L\mathbf{z})\mathbf{z}^\top \quad (20)$$

The gradient update rule for the lifted dictionary D_L is:

$$D_L^{(k+1)} = D_L^{(k)} - \eta_L \frac{\partial \mathcal{L}}{\partial D_L^{(k)}} = D_L^{(k)} + \eta_L \mathbf{P}^\top (\mathbf{x} - \mathbf{P} D_L \mathbf{z})(\mathbf{z})^\top \quad (21)$$

To understand the learning dynamics in the original space, we first incorporate the underlying model from L-SAEs into SAE using the relation $D' = \mathbf{P} D_L$. Then, we derive the update rule for the effective dictionary, D' . Left-multiplying the update for $D_L^{(k+1)}$ by \mathbf{P} , we have:

$$D'^{(k+1)} = D'^{(k)} + \eta_L (\mathbf{P} \mathbf{P}^\top) (\mathbf{x} - D'^{(k)} \mathbf{z})(\mathbf{z})^\top \quad (22)$$

In our specific architecture, we constrain the projection matrix to be the transpose of the lifting matrix such that $\mathbf{P} = \mathbf{L}^\top$. Substituting this into the update rules yields:

$$D_L^{(k+1)} = D_L^{(k)} + \eta_L \mathbf{L} (\mathbf{x} - \mathbf{L}^\top D_L \mathbf{z})(\mathbf{z})^\top \quad (23)$$

$$D'^{(k+1)} = D'^{(k)} + \eta_L (\mathbf{L}^\top \mathbf{L}) (\mathbf{x} - D'^{(k)} \mathbf{z})(\mathbf{z})^\top \quad (24)$$

Hence, when $\mathbf{L}^\top \mathbf{L} = \mathbf{I}$, the lifted-SAE shows equivalent learning dynamics as the standard SAE for model recovery. ■

Proposition C.3 (Architectural Inference Equivalence of Lifting in SAE-CNN). *The architectural inference of a SAE-CNN is equivalent to a lifted SAE-CNN (L-SAE-CNN) if the projection is tied to the lifting operator ($\mathbf{P} = \mathbf{L}^\top$), and the lifting operator is orthogonal ($\mathbf{L}^\top \mathbf{L} = \mathbf{I}$), i.e., under the same learned model $D_c = \mathbf{P} D_{L,c}$, the representation dynamics and output of the networks are equivalent.*

Proof. We provide the proof for the sparse convolutional generative model case when the encoder implements a proximal gradient descent type of operation in an unrolled learning setting (e.g., 9). For the SAE-CNN, the representation refinement for the c -th feature map at every encoder layer follows:

$$\mathbf{z}_{c,t+1} = \mathcal{R} \left(\mathbf{z}_{c,t} - \alpha \left(\sum_{i=1}^C D_i * \mathbf{z}_{i,t} - \mathbf{x} \right) * D_c \right) \quad (25)$$

By construction, we incorporate the underlying model from the lifted-SAE-CNN to the standard SAE-CNN: $D_c^{(k)} = \mathbf{P} D_{L,c}^{(k)}$, and re-write the encoder using the adjoint property:

$$\mathbf{z}_{c,t+1} = \mathcal{R} \left(\mathbf{z}_{c,t} - \alpha \left(\mathbf{P}^\top \left[\left(\sum_{i=1}^C \mathbf{P} D_{L,i} * \mathbf{z}_{i,t} \right) - \mathbf{x} \right] * D_{L,c} \right) \right) \quad (26)$$

$$\mathbf{z}_{c,t+1} = \mathcal{R} \left(\mathbf{z}_{c,t} - \alpha \left(\sum_{i=1}^C (\mathbf{P}^\top \mathbf{P}) D_{L,i} * \mathbf{z}_{i,t} - \mathbf{P}^\top \mathbf{x} \right) * D_{L,c} \right) \quad (27)$$

Using the assumption on the lifting-projection,

$$\mathbf{z}_{c,t+1} = \mathcal{R} \left(\mathbf{z}_{c,t} - \alpha \left(\sum_{i=1}^C D_{L,i} * \mathbf{z}_{i,t} - \mathbf{L} \mathbf{x} \right) * D_{L,c} \right) \quad (28)$$

This final expression is the iterative encoder update for \mathbf{z}_c in the lifted space, where the dictionary is D_L and the input is lifted by \mathbf{L} . This completes the proof of architectural inference equivalence for SAE-CNN and L-SAE-CNN. ■

Proposition C.4 (Training Dynamics of Lifted SAE-CNN). *The training dynamics of the lifted-SAE-CNN (L-SAE-CNN)*

$D_{L,c}^{(k+1)} = D_{L,c}^{(k)} + \eta_L \mathbf{L} \left(\mathbf{x} - \mathbf{L}^\top \left(\sum_{i=1}^C D_{L,i}^{(k)} * \mathbf{z}_{i,t} \right) \right) * \mathbf{z}_{c,t}$, with a lifting operator \mathbf{L} and projection \mathbf{P} , has the effective update in the original space, expressed as: $D_c^{(k+1)} = D_c^{(k)} + \eta_L (\mathbf{L}^\top \mathbf{L}) \left(\mathbf{x} - \sum_{i=1}^C D_i^{(k)} * \mathbf{z}_{i,t} \right) * \mathbf{z}_{c,t}$, where $\mathbf{L}^\top \mathbf{L}$ acts

as a preconditioner, potentially accelerating learning by inducing a more isotropic update. If the architectures satisfy the architectural inference equivalence condition (Proposition C.3), then the dynamics become equivalent to that of a SAE-CNN:

$$\mathbf{D}_c^{(k+1)} = \mathbf{D}_c^{(k)} + \eta \left(\mathbf{x} - \sum_{i=1}^C \mathbf{D}_i^{(k)} * \mathbf{z}_{i,t} \right) * \mathbf{z}_{c,t}.$$

Proof. For the SAE-CNN, we learn a dictionary \mathbf{D} by minimizing the reconstruction loss for the data sample \mathbf{x} . The loss function is:

$$\mathcal{L}(\mathbf{D}) = \frac{1}{2} \left\| \mathbf{x} - \sum_{c=1}^C \mathbf{D}_c * \mathbf{z}_c \right\|_2^2 \quad (29)$$

The gradient of the loss with respect to the c -th kernel \mathbf{D}_c is:

$$\frac{\partial \mathcal{L}}{\partial \mathbf{D}_c} = - \left(\mathbf{x} - \sum_{i=1}^C \mathbf{D}_i * \mathbf{z}_i \right) * \mathbf{z}_c \quad (30)$$

where $*$ denotes cross-correlation.

The analytic gradient update, given \mathbf{z} , for \mathbf{D}_c at iteration k with a learning rate η is:

$$\mathbf{D}_c^{(k+1)} = \mathbf{D}_c^{(k)} + \eta \left(\mathbf{x} - \sum_{i=1}^C \mathbf{D}_i^{(k)} * \mathbf{z}_{i,t} \right) * \mathbf{z}_{c,t} \quad (31)$$

For L-SAE-CNN, we learn a dictionary $\mathbf{D}_L = \{\mathbf{D}_{L,c}\}_{c=1}^C$ that operates in a higher-dimensional lifted space. The input signal \mathbf{x} is first lifted by \mathbf{L} (acts on the channel dimension) to $\tilde{\mathbf{x}}$ and the reconstruction $\hat{\mathbf{x}}$ is obtained by projecting the lifted reconstruction $\hat{\mathbf{x}} = \sum_c \mathbf{D}_{L,c} * \mathbf{z}_c$ back by \mathbf{P} .

The loss function is defined in the original data space:

$$\mathcal{L}(\mathbf{D}) = \frac{1}{2} \left\| \mathbf{x} - \mathbf{P} \left(\sum_{c=1}^C \mathbf{D}_{L,c} * \mathbf{z}_c \right) \right\|_2^2 \quad (32)$$

The analytic gradient of the loss, given \mathbf{z} , with respect the c -th lifted kernel $\mathbf{D}_{L,c}$ is:

$$\frac{\partial \mathcal{L}}{\partial \mathbf{D}_{L,c}} = -\mathbf{P}^\top \left(\mathbf{x} - \mathbf{P} \left(\sum_{i=1}^C \mathbf{D}_{L,i} * \mathbf{z}_i \right) \right) * \mathbf{z}_c \quad (33)$$

The gradient update rule for $\mathbf{D}_{L,c}$ is:

$$\mathbf{D}_{L,c}^{(k+1)} = \mathbf{D}_{L,c}^{(k)} + \eta_L \mathbf{P}^\top \left(\mathbf{x} - \mathbf{P} \left(\sum_{i=1}^C \mathbf{D}_{L,i}^{(k)} * \mathbf{z}_{i,t} \right) \right) * \mathbf{z}_{c,t} \quad (34)$$

To understand the learning dynamics in the original space, we derive the update rule for the effective dictionary $\mathbf{D}'_c = \mathbf{P} \mathbf{D}_{L,c}$, i.e., the case where both frameworks contain the same underlying model but in a different form. Left-multiplying the update for $\mathbf{D}_{L,c}^{(k+1)}$ update rule by \mathbf{P} , we get:

$$\mathbf{D}'_c{}^{(k+1)} = \mathbf{D}'_c{}^{(k)} + \eta_L (\mathbf{P} \mathbf{P}^\top) \left(\mathbf{x} - \sum_{i=1}^C \mathbf{D}'_i{}^{(k)} * \mathbf{z}_{i,t} \right) * \mathbf{z}_{c,t} \quad (35)$$

In our specific architecture, we constrain the projection matrix to be the transpose of the lifting matrix such that $\mathbf{P} = \mathbf{L}^\top$. Substituting this into the update rules yields:

$$\mathbf{D}'_c{}^{(k+1)} = \mathbf{D}'_c{}^{(k)} + \eta_L \mathbf{L} \left(\mathbf{x} - \mathbf{L}^\top \left(\sum_{i=1}^C \mathbf{D}'_i{}^{(k)} * \mathbf{z}_{i,t} \right) \right) * \mathbf{z}_{c,t} \quad (36)$$

$$\mathbf{D}'_c{}^{(k+1)} = \mathbf{D}'_c{}^{(k)} + \eta_L (\mathbf{L}^\top \mathbf{L}) \left(\mathbf{x} - \sum_{i=1}^C \mathbf{D}'_i{}^{(k)} * \mathbf{z}_{i,t} \right) * \mathbf{z}_{c,t} \quad (37)$$

Hence, when $\mathbf{L}^\top \mathbf{L} = \mathbf{I}$, the lifted-SAE-CNN shows equivalent learning dynamics as the standard SAE-CNN for model recovery. \blacksquare

Proposition 3.5 (Training Dynamics of Lifted SAE-FNO). *The training dynamics of the Lifted-SAE-FNO (L-SAE-FNO)'s frequency domain weights $\mathbf{W}_{L,c}^{(k+1)} = \mathbf{W}_{L,c}^{(k)} + \frac{\eta_L}{\sqrt{M}} \mathcal{F}(\mathbf{L}(\mathbf{x} - \hat{\mathbf{x}}^{(k)})) \odot \mathcal{F}(\mathbf{z}_{c,k})$, with lifting operator \mathbf{L} and projection \mathbf{P} , has an effective update in the original space, expressed as: $\mathbf{D}'_c{}^{(k+1)} = \mathbf{D}'_c{}^{(k)} + \frac{\eta_L}{M} ((\mathbf{L}^\top \mathbf{L})(\mathbf{x} - \hat{\mathbf{x}}^{(k)})) * \mathbf{z}_{c,t}$, where $\mathbf{L}^\top \mathbf{L}$ acts as a preconditioner, potentially. If the architectures satisfy the architectural inference equivalence condition (Proposition C.8), then the dynamics is equivalent to that of an SAE-FNO: $\mathbf{D}'_c{}^{(k+1)} = \mathbf{D}'_c{}^{(k)} + \frac{\eta}{M} \left(\mathbf{x} - \frac{1}{\sqrt{M}} \mathcal{F}^{-1} \left(\sum_{i=1}^C \mathcal{F}(\mathbf{D}'_i{}^{(k)}) \odot \mathcal{F}(\mathbf{z}_{i,k}) \right) \right) * \mathbf{z}_{c,k}$.*

Proof. For the SAE-FNO, we learn frequency-domain weights $\mathbf{W}_c = \mathcal{F} \mathbf{D}_c$ by minimizing the reconstruction loss for the data sample \mathbf{x} . Taking normalization into account, the reconstruction operator is $\hat{\mathbf{x}} = \mathcal{G}_{\mathbf{W}}(\mathbf{z}) = \frac{1}{\sqrt{M}} \mathcal{F}^{-1} \left(\sum_{c=1}^C \mathbf{W}_c \cdot (\mathcal{F} \mathbf{z}_c) \right)$, where $\mathbf{W}_c = \mathcal{F} \mathbf{D}_c$, where M is the number of modes. The loss function is:

$$\mathcal{L}(\mathbf{W}) = \frac{1}{2} \mathbb{E}_{\mathbf{z} \sim \mu} \left[\|\mathbf{x} - \mathcal{G}_{\mathbf{W}}(\mathbf{z})\|_{\mathcal{X}}^2 \right] \quad (38)$$

where $\mathbf{x} = \mathcal{G}_{\mathcal{D}^*}(\mathbf{z})$ is the ground-truth signal.

The gradient of the loss with respect to the c -th frequency-domain kernel \mathbf{W}_c is:

$$\frac{\partial \mathcal{L}}{\partial \mathbf{W}_c} = -\frac{1}{\sqrt{M}} \mathcal{F}(\mathbf{x} - \hat{\mathbf{x}}) \odot \mathcal{F}(\mathbf{z}_c) \quad (39)$$

The analytic gradient update, given \mathbf{z} , for \mathbf{W}_c at iteration k with a learning rate η is:

$$\mathbf{W}_c^{(k+1)} = \mathbf{W}_c^{(k)} + \frac{\eta}{\sqrt{M}} \mathcal{F}(\mathbf{x} - \hat{\mathbf{x}}^{(k)}) \odot \mathcal{F}(\mathbf{z}_{c,k}) \quad (40)$$

Applying the inverse Fourier transform and the cross-correlation theorem, we obtain the effective update rule for the spatial dictionary \mathbf{D}'_c :

$$\mathbf{D}'_c{}^{(k+1)} = \mathbf{D}'_c{}^{(k)} + \frac{\eta}{M} (\mathbf{x} - \hat{\mathbf{x}}^{(k)}) * \mathbf{z}_{c,t} = \mathbf{D}'_c{}^{(k)} + \frac{\eta}{M} \left(\mathbf{x} - \frac{1}{\sqrt{M}} \mathcal{F}^{-1} \sum_{i=1}^C \mathcal{F} \mathbf{D}'_i{}^{(k)} \odot \mathcal{F} \mathbf{z}_{i,k} \right) * \mathbf{z}_{c,t} \quad (41)$$

In the lifted scenario, we learn a dictionary $\mathbf{W}_L = \{\mathbf{W}_{L,c}\}_{c=1}^C$ that operates in a higher -dimensional lifted frequency domain. The input signal \mathbf{x} is lifted by \mathbf{L} , and the reconstruction is projected back by \mathbf{P} . The reconstruction operator is $\hat{\mathbf{x}} = \mathbf{P}(\mathcal{G}_{\mathbf{W}_L}(\mathbf{z})) = \mathbf{P} \left(\frac{1}{\sqrt{M}} \mathcal{F}^{-1} \left(\sum_{c=1}^C \mathbf{W}_{L,c} \odot \mathcal{F}(\mathbf{z}_c) \right) \right)$.

The loss function is defined in the original spatial space:

$$\mathcal{L}(\mathbf{W}) = \frac{1}{2} \mathbb{E}_{\mathbf{z} \sim \mu} \left[\|\mathbf{x} - \mathbf{P}(\mathcal{G}_{\mathbf{W}_L}(\mathbf{z}))\|_{\mathcal{X}}^2 \right] \quad (42)$$

The gradient of the loss with respect to $\mathbf{W}_{L,c}$, given \mathbf{z} , is:

$$\frac{\partial \mathcal{L}}{\partial \mathbf{W}_{L,c}} = -\frac{1}{\sqrt{M}} \mathcal{F} \left(\mathbf{P}^\top (\mathbf{x} - \hat{\mathbf{x}}^{(k)}) \right) \odot \mathcal{F}(\mathbf{z}_c) \quad (43)$$

The analytic gradient update for $\mathbf{W}_{L,c}$ at iteration k with a learning rate η_L is:

$$\mathbf{W}_{L,c}^{(k+1)} = \mathbf{W}_{L,c}^{(k)} + \frac{\eta_L}{\sqrt{M}} \mathcal{F} \left(\mathbf{P}^\top \left(\mathbf{x} - \hat{\mathbf{x}}^{(k)} \right) \right) \odot \mathcal{F}(\mathbf{z}_{c,t}) \quad (44)$$

To understand the learning dynamics in the original spatial-domain, we derive the update rule for the effective lifted spatial dictionary $\mathbf{D}'_{L,c}$. Taking the inverse Fourier, we get:

$$\mathbf{D}'_{L,c}{}^{(k+1)} = \mathbf{D}'_{L,c}{}^{(k)} + \frac{\eta_L}{M} \left(\mathbf{P}^\top \left(\mathbf{x} - \hat{\mathbf{x}}^{(k)} \right) \right) \star \mathbf{z}_{c,t} \quad (45)$$

We also derive the update rule for the effective spatial dictionary in the original space \mathbf{D}'_c . Left-multiplying the update for $\mathbf{D}'_{L,c}$ by \mathbf{P} , we have:

$$\mathbf{D}'_c{}^{(k+1)} = \mathbf{D}'_c{}^{(k)} + \frac{\eta_L}{M} \left((\mathbf{P}\mathbf{P}^\top) \left(\mathbf{x} - \hat{\mathbf{x}}^{(k)} \right) \right) \star \mathbf{z}_{c,t} \quad (46)$$

In our specific architecture, we constrain the projection matrix to be the transpose of the lifting matrix such that $\mathbf{P} = \mathbf{L}^\top$. Substituting this into the update rules yields:

$$\mathbf{W}_{L,c}^{(k+1)} = \mathbf{W}_{L,c}^{(k)} + \frac{\eta_L}{\sqrt{M}} \mathcal{F} \left(\mathbf{L} \left(\mathbf{x} - \hat{\mathbf{x}}^{(k)} \right) \right) \odot \mathcal{F}(\mathbf{z}_{c,t}) \quad (47)$$

$$\mathbf{D}'_{L,c}{}^{(k+1)} = \mathbf{D}'_{L,c}{}^{(k)} + \frac{\eta_L}{M} \left(\mathbf{L} \left(\mathbf{x} - \hat{\mathbf{x}}^{(k)} \right) \right) \star \mathbf{z}_{c,t} \quad (48)$$

$$\mathbf{D}'_c{}^{(k+1)} = \mathbf{D}'_c{}^{(k)} + \frac{\eta_L}{M} \left((\mathbf{L}^\top \mathbf{L}) \left(\mathbf{x} - \hat{\mathbf{x}}^{(k)} \right) \right) \star \mathbf{z}_{c,t} \quad (49)$$

Substituting for $\hat{\mathbf{x}}^{(k)}$, the full effective spatial-domain update is:

$$\mathbf{D}'_c{}^{(k+1)} = \mathbf{D}'_c{}^{(k)} + \frac{\eta_L}{M} \left((\mathbf{L}^\top \mathbf{L}) \left(\mathbf{x} - \frac{1}{\sqrt{M}} \mathcal{F}^{-1} \left(\sum_{i=1}^C \mathcal{F}(\mathbf{D}'_i{}^{(k)}) \odot \mathcal{F}(\mathbf{z}_{i,t}) \right) \right) \right) \star \mathbf{z}_{c,t} \quad (50)$$

Hence, when $\mathbf{L}^\top \mathbf{L} = \mathbf{I}$, the lifted-SAE-FNO shows equivalent learning dynamics as the standard SAE-FNO for model recovery. \blacksquare

Proposition C.5 (Architectural Inference Equivalence of SAE-CNN and SAE-FNO). *The architectural inference of an SAE-CNN is equivalent to a sparse autoencoder neural operator (SAE-NO) if the integral operator of SAE-FNO and parameters of SAEs are defined as a convolution where the SAE-FNO's frequency-domain weights \mathbf{W}_c are the Fourier transform of SAE-CNN's spatial domain kernels: $\mathbf{W}_c = \mathcal{F}\mathbf{D}_c$.*

Proof. We provide the proof for an encoder that implements a proximal gradient descent type of operation in an unrolled learning setting. For the SAE-CNN, the representation refinement for the c -th feature map at every encoder layer follows:

$$\mathbf{z}_{c,t+1} = \mathcal{R} \left(\mathbf{z}_{c,t} - \alpha \left(\sum_{i=1}^C \mathbf{D}_i \star \mathbf{z}_{i,t} - \mathbf{x} \right) \star \mathbf{D}_c \right) \quad (51)$$

By construction, we incorporate the underlying model from the SAE-FNO to the SAE-CNN: $\mathbf{W}_c = \mathcal{F}\mathbf{D}_c$, and re-write the gradient of the encoder using Correlation and Convolution Theorems:

$$\mathcal{F}^{-1} \left(\mathcal{F} \left(\sum_{i=1}^C \mathbf{D}_i \star \mathbf{z}_{i,t} - \mathbf{x} \right) \odot \mathcal{F}\mathbf{D}_c^H \right) = \mathcal{F}^{-1} \left(\sum_{i=1}^C \mathbf{W}_i \odot \mathcal{F}\mathbf{z}_{i,t} - \mathcal{F}\mathbf{x} \right) \odot (\mathbf{W}_c)^H \quad (52)$$

Substituting this back into Equation (51) gives:

$$\mathbf{z}_{c,t+1} = \mathcal{R} \left(\mathbf{z}_{c,t} - \alpha \mathcal{F}^{-1} \left(\left(\sum_{i=1}^C \mathbf{W}_i \odot \mathcal{F}\mathbf{z}_{i,t} \right) - \mathcal{F}\mathbf{x} \right) \odot (\mathbf{W}_c)^H \right) \quad (53)$$

This final expression is the SAE-FNO’s iterative encoder update for z_c in the spectral domain, where the dictionary is \mathbf{W} . This completes the proof of architectural inference equivalence between SAE-CNN and SAE-FNO. ■

Proposition C.6 (Training Dynamics of SAE-CNN and SAE-FNO). *The training dynamics of the SAE-FNO’s frequency-domain weights $\mathbf{W}_c^{(k+1)} = \mathbf{W}_c^{(k)} + \frac{\eta_L}{\sqrt{M}} \mathcal{F}(\mathbf{x} - \hat{\mathbf{x}}^{(k)}) \odot \mathcal{F}(z_{c,t})$ has an effective update in the original space, expressed as: $\mathbf{D}_c'^{(k+1)} = \mathbf{D}_c'^{(k)} + \frac{\eta}{M} (\mathbf{x} - \hat{\mathbf{x}}^{(k)}) \star z_{c,t}$. If the architectures satisfy the architectural inference equivalence condition (Proposition C.5), then the dynamics is equivalent to that of a SAE-CNN: $\mathbf{D}_c^{(k+1)} = \mathbf{D}_c^{(k)} + \eta \left(\mathbf{x} - \sum_{i=1}^C \mathbf{D}_i^{(k)} \star z_{i,t} \right) \star z_{c,t}$.*

Proof. For a standard SAE-CNN, we learn a dictionary \mathbf{D} by minimizing the reconstruction loss for the data sample \mathbf{x} . The loss function is:

$$\mathcal{L}(\mathbf{D}) = \frac{1}{2} \left\| \mathbf{x} - \sum_{c=1}^C \mathbf{D}_c \star z_c \right\|_2^2 \quad (54)$$

The gradient of the loss with respect to the c -th kernel \mathbf{D}_c is:

$$\frac{\partial \mathcal{L}}{\partial \mathbf{D}_c} = - \left(\mathbf{x} - \sum_{i=1}^C \mathbf{D}_i \star z_i \right) \star z_c \quad (55)$$

where \star denotes cross-correlation.

The analytic gradient update, given z , for \mathbf{D}_c at iteration k with a learning rate η is:

$$\mathbf{D}_c^{(k+1)} = \mathbf{D}_c^{(k)} + \eta \left(\mathbf{x} - \sum_{i=1}^C \mathbf{D}_i^{(k)} \star z_{i,t} \right) \star z_{c,t} \quad (56)$$

For a standard SAE-FNO, we learn frequency-domain weights $\mathbf{W}_c = \mathcal{F}\mathbf{D}_c$ by minimizing the reconstruction loss for the data sample \mathbf{x} . Taking normalization into account, the reconstruction operator is $\hat{\mathbf{x}} = \mathcal{G}_{\mathbf{W}}(z) = \frac{1}{\sqrt{M}} \mathcal{F}^{-1} \left(\sum_{c=1}^C \mathbf{W}_c \cdot (\mathcal{F}z_c) \right)$, where $\mathbf{W}_c = \mathcal{F}\mathbf{D}_c$, where M is the number of modes. The loss function is:

$$\mathcal{L}(\mathbf{W}) = \frac{1}{2} \mathbb{E}_{z \sim \mu} \left[\|\mathbf{x} - \mathcal{G}_{\mathbf{W}}(z)\|_{\mathcal{X}}^2 \right] \quad (57)$$

where $\mathbf{x} = \mathcal{G}_{D^*}(z)$ is the ground-truth signal.

The gradient of the loss with respect to the c -th frequency-domain kernel \mathbf{W}_c is:

$$\frac{\partial \mathcal{L}}{\partial \mathbf{W}_c} = - \frac{1}{\sqrt{M}} \mathcal{F}(\mathbf{x} - \hat{\mathbf{x}}) \odot \mathcal{F}(z_c) \quad (58)$$

The analytic gradient update, given z , for \mathbf{W}_c at iteration k with a learning rate η is:

$$\mathbf{W}_c^{(k+1)} = \mathbf{W}_c^{(k)} + \frac{\eta}{\sqrt{M}} \mathcal{F}(\mathbf{x} - \hat{\mathbf{x}}^{(k)}) \odot \mathcal{F}(z_{c,k}) \quad (59)$$

Applying the inverse Fourier transform and the cross-correlation theorem, we obtain the effective update rule for the spatial dictionary \mathbf{D}_c' :

$$\mathbf{D}_c'^{(k+1)} = \mathbf{D}_c'^{(k)} + \frac{\eta}{M} (\mathbf{x} - \hat{\mathbf{x}}^{(k)}) \star z_{c,t} \quad (60)$$

This is equivalent to the gradient update of SAE-CNN with a scaling factor of $\frac{1}{M}$ on the learning rate, which arises from the inverse Fourier normalization conventions. ■

Proposition C.7 (Architectural Inference Equivalence of L-SAE-CNN and L-SAE-FNO). *The architectural inference of a L-SAE-CNN is equivalent to a L-SAE-FNO if the integral operator of L-SAE-FNO and parameters of SAEs are defined as a convolution where the L-SAE-FNO’s lifted frequency-domain weights $\mathbf{W}_{L,c}$ are the Fourier transform of L-SAE-CNN’s lifted spatial domain kernels: $\mathbf{W}_{L,c} = \mathcal{F}\mathbf{D}_{L,c}$.*

Proof. We provide proof for an encoder that implements a proximal gradient descent type of operation in an unrolled learning setting. For the L-SAE-CNN, the representation refinement for the c -th feature map at every encoder layer follows:

$$\mathbf{z}_{c,t+1} = \mathcal{R} \left(\mathbf{z}_{c,t} - \alpha \left(\sum_{i=1}^C \mathbf{D}_{L,i} * \mathbf{z}_{i,t} - \mathbf{L}\mathbf{x} \right) * \mathbf{D}_{L,c} \right) \quad (61)$$

By construction, we incorporate the underlying model from the L-SAE-FNO to the L-SAE-CNN: $\mathbf{W}_{L,c} = \mathcal{F}\mathbf{D}_{L,c}$, and re-write the gradient of the encoder using Correlation and Convolution Theorems:

$$\mathcal{F}^{-1} \left(\mathcal{F} \left(\sum_{i=1}^C \mathbf{D}_{L,i}^{(k)} * \mathbf{z}_{i,t} - \mathbf{L}\mathbf{x} \right) \odot \mathcal{F}\mathbf{D}_{L,c}^H \right) = \mathcal{F}^{-1} \left(\sum_{i=1}^C \mathbf{W}_{L,i}^{(k)} \odot \mathcal{F}\mathbf{z}_{i,t} - \mathcal{F}(\mathbf{L}\mathbf{x}) \right) \odot (\mathbf{W}_{L,c})^H \quad (62)$$

Substituting this back into Equation (61) gives:

$$\mathbf{z}_{c,t+1} = \mathcal{R} \left(\mathbf{z}_{c,t} - \alpha \mathcal{F}^{-1} \left[\left(\left(\sum_{i=1}^C \mathbf{W}_{L,i} \odot \mathcal{F}(\mathbf{z}_{i,t}) \right) - \mathcal{F}(\mathbf{L}\mathbf{x}) \right) \odot (\mathbf{W}_{L,c})^H \right] \right) \quad (63)$$

This final expression is the L-SAE-FNO's iterative update for \mathbf{z}_c in the lifted spectral domain, where the dictionary is $\mathbf{W}_{L,c}$. This completes the proof of architectural inference equivalence between L-SAE-CNN and L-SAE-FNO. ■

Proposition C.8 (The Architectural Inference of L-SAE-FNO reduced to SAE-FNO). *The architectural inference of an SAE-FNO is equivalent to a L-SAE-FNO if the projection is tied to the lifting operator ($\mathbf{P} = \mathbf{L}^\top$), and the lifting operator is orthogonal ($\mathbf{L}^\top \mathbf{L} = \mathbf{I}$), i.e., under the same learned model $\mathbf{W}_c = \mathbf{P}\mathbf{W}_{L,c}$, the representation dynamics and output of the networks are equivalent.*

Proof. We prove this equivalence by establishing a chain of architectural inference equivalences that connects the SAE-FNO to the Lifted SAE-FNO, leveraging the propositions previously established:

1. From Proposition C.5, the architectural inference of an SAE-FNO is equivalent to a SAE-CNN.
2. From Proposition C.3, the architectural inference of a SAE-CNN is equivalent to L-SAE-CNN.
3. From Proposition C.7, the architectural inference of a L-SAE-CNN is equivalent to a L-SAE-FNO.

By the transitive property of these equivalences, we can establish a direct architectural inference equivalence between SAE-FNO and L-SAE-FNO under the same lifting-projection conditions. This completes the proof. ■

Proposition C.9 (Training Dynamics of SAE-FNO). *Consider an SAE-FNO whose integral operator is implemented as a convolution, with frequency-domain weights \mathbf{W}_c defined as the Fourier transform of the Conv-SAE's spatial kernels, i.e., $\mathbf{W}_c = \mathcal{F}\mathbf{D}_c$. The training dynamics of the SAE-FNO are then expressed as: $\mathbf{D}_c^{(k+1)} = \mathbf{D}_c^{(k)} + \frac{\eta}{M} (\mathbf{x} - \frac{1}{\sqrt{M}} \mathcal{F}^{-1} [\sum_{i=1}^C \mathcal{F}\mathbf{D}_i^{(k)} \odot \mathcal{F}\mathbf{z}_i]) * \mathbf{z}_c$ where M is the full number of modes, \odot denotes element-wise multiplication, and $*$ denotes correlation. If the SAE-FNO's filters span the full frequency range and are constrained to have the same spatial support as in the Conv-SAE, then its dynamics reduce to those of the Conv-SAE (see Proposition C.6).*